Institute, for their valuable advice and comments. We would also like to thank the laboratory members of Toyama Chemical Co. Ltd. for supplying the compounds in the study. Finally, we would like to thank Ms. Mary Phillips and Ms. Yumi Fujiuji for preparing the manuscript.

References

Balzarini J (2004) Current status of the non-nucleoside reverse transcriptase inhibitors of human immunodeficiency virus type 1. *Current Topics in Medicinal Chemistry* **4**:921–944.

Burke CJ, Sanyal G, Bruner MW, Ryan JA, LaFemina RL, Robbins HL, Zeft AS, Middaugh CR & Cordingley MG (1992) Structural implications of spectroscopic characterization of a putative zinc finger peptide from HIV-1 integrase. *The Journal of Biological Chemistry* **267**:9639–9644.

Cain BF, Baguley BC & Denny WA (1978) Potential antitumor agent. 28. deoxyribonucleic acid polyintercalating agents. *Journal of Medicinal Chemistry* **21**:658–668.

Carrasco C, Vezin H, Wilson WD, Ren J, Chaires JB & Bailly C (2001) DNA binding properties of the indolocarbazole antitumor drug NB-506. *Anticancer Drug Design* **16**:99–107.

Chun TW, Finzi D, Margolick J, Chadwick K, Schwartz D & Siliciano RF (1995) *In vivo* fate of HIV-1-infected T cells: quantitative analysis of the transition to stable latency. *Nature Medicine* **1**:1284–1290.

Craigie R, Hickman AB & Engelman A (1995) Integrase. in *HIV: A Practical Approach – Volume 2: Biochemistry, Molecular Biology, and Drug Discovery*, pp. 53–71. Edited by J Karn. New York: Oxford University Press.

Dayam R & Neamati N (2003) Small-molecule HIV-1 integrase inhibitors: the 2001–2002 update. *Current Pharmacology Design* **9**:1789–1802.

De Clercq E (1992) HIV inhibitors targeted at the reverse transcriptase. *AIDS Research and Human Retroviruses* **8**:119–134.

Dziegielewski J, Slusarski B, Konitz A, Skladanowski A & Konopa J (2002) Intercalation of imidazoacridinones to DNA and its relevance to cytotoxic and antitumor activity. *Biochemical Pharmacology* **63**:1653–1662.

Engelman A & Craigie R (1992) Identification of conserved amino acid residues critical for human immunodeficiency virus type 1 integrase function *in vitro*. *Journal of Virology* **66**:6361–6369.

Engelman A, Englund G, Orenstein JM, Martin MA & Craigie R (1995) Multiple effects of mutations in human immunodeficiency virus type 1 integrase on viral replication. *Journal of Virology* **69**:2729–2736.

Engelman A, Hickman AB & Craigie R (1994) The core and carboxyl-terminal domains of the integrase protein of human immunodeficiency virus type 1 each contribute to nonspecific DNA binding. *Journal of Virology* **68**:5911–5917.

Facompre M, Carrasco C, Colson P, Houssier C, Chisholm JD, Van Vranken DL & Bailly C (2002) DNA binding and topoisomerase I poisoning activities of novel disaccharide indolocarbazoles. *Molecular Pharmacology* **62**:1215–1227.

Fukui K & Tanaka K (1996) The acridine ring selectively intercalated into a DNA helix at various types of abasic sites: double strand formation and photophysical properties. *Nucleic Acids Research* **24**:3962–3967.

Furusaki A, Hashiba N, Matsumoto T, Hirano A, Iwai Y & Omura S (1978) X-ray crystal structure of staurosporine: a new alkaloid from a Streptomyces strains. *Journal of the Chemical Society. Chemical Communications* 800–801.

Furusaki A, Hashiba N, Matsumoto T, Hirano A, Iwai Y & Omura S (1982) The crystal and molecular structure of staurosporine, a new alkaloid from a Streptomyces strains. *Bulletin of the Chemical Society of Japan* **55**:3681–3685.

Goldgur Y, Craigie R, Cohen GH, Fujiwara T, Yoshinaga T, Fujishita T, Sugimoto H, Endo T, Murai H & Davies DR (1999) Structure of the HIV-1 integrase catalytic domain complexed with an inhibitor: a platform for antiviral drug design. *Proceedings of the National Academy of Sciences, USA* **96**:13040–13043.

Grobler JA, Stillmock K, Hu B, Witmer M, Felock P, Espeseth AS, Wolfe A, Egbertson M, Bourgeois M, Melamed J, Wai JS, Young S, Vacca J & Hazuda DJ (2002) Diketo acid inhibitor mechanism and HIV-1 integrase: implications for metal binding in the active site of phosphotransferase enzymes. *Proceedings of the National Academy of Sciences USA* **99**:6661–6666.

Hazuda DJ, Anthony NJ, Gomez RP, Jolly SM, Wai JS, Zhuang L, Fisher TE, Embrey M, Guare JP, Jr., Egbertson MS, Vacca JP, Huff JR, Felock PJ, Witmer MV, Stillmock KA, Danovich R, Grobler J, Miller MD, Espeseth AS, Jin L, Chen IW, Lin JH, Kassahun K, Ellis JD, Wong BK, Xu W, Pearson PG, Schleif WA, Cortese R, Emini E, Summa V, Holloway MK & Young SD (2004) A naphthyridine carboxamide provides evidence for discordant resistance between mechanistically identical inhibitors of HIV-1 integrase. *Proceedings of the National Academy of Sciences USA* **101**:11233–11238.

Hazuda DJ, Felock P, Witmer M, Wolfe A, Stillmock K, Grobler JA, Espeseth A, Gabryelski L, Schleif W, Blau C & Miller MD (2000) Inhibitors of strand transfer that prevent integration and inhibit HIV-1 replication in cells. *Science* **287**:646–650.

Imamichi T (2004) Action of anti-HIV drugs and resistance: reverse transcriptase inhibitors and protease inhibitors. *Current Pharmaceutical Design* **10**:4039–4053.

Johnson AA, Marchand C & Pommier Y (2004) HIV-1 integrase inhibitors: a decade of research and two drugs in clinical trial. *Current Topics in Medicinal Chemistry* **4**:1059–1077.

Khan E, Mack JP, Katz RA, Kulkosky J & Skalka AM (1991) Retroviral integrase domains: DNA binding and the recognition of LTR sequences. *Nucleic Acids Research* **19**:851–860.

Kohl NE, Emini EA, Schleif WA, Davis LJ, Heimbach JC, Dixon RA, Scolnick EM & Sigal IS (1988) Active human immunodeficiency virus protease is required for viral infectivity. *Proceedings of National Academy of Sciences USA* **85**:4686–4690.

LaFemina RL, Schneider CL, Robbins HL, Callahan PL, LeGrow K, Roth E, Schleif WA & Emini EA (1992) Requirement of active human immunodeficiency virus type 1 integrase enzyme for productive infection of human T-lymphoid cells. *Journal of Virology* **66**:7414–7419.

Long BH, Rose WC, Vyas DM, Matson JA & Forenza S (2002) Discovery of antitumor indolocarbazoles: rebeccamycin, NSC 655649, and fluoroindolocarbazoles. *Current Medicinal Chemistry. Anti-Cancer Agents* **2**:255–266.

Marotto A, Kim YS, Schulze E & Pindur U (2002) New indolocarbazoles as antitumour active compounds: evaluation of the target by experimental and theoretical studies. *Pharmazie* **57**:194–197.

Oka S, Kodama M, Takeda H, Tomizuka N & Suzuki H (1986) Staurosporine, a potent platelet aggregation inhibitor form a *Streptomyces* species. *Agricultural and Biological Chemistry* **50**:2723–2727.

Omura S, Iwai Y, Hirano A, Nakagawa A, Awaya J, Tsuchya H, Takahashi Y & Masuma R (1977) A new alkaloid AM-2282 of *Streptomyces* origin. Taxonomy, fermentation, isolation and preliminary characterization. *The Journal of Antibiotics (Tokyo)* **30**:275–282.

Pluymers W, Pais G, Van Maele B, Pannecouque C, Fikkert V, Burke TR, Jr., De Clercq E, Witvrouw M, Neamati N & Debyser Z (2002) Inhibition of human immunodeficiency virus type 1 integration by diketo derivatives. *Antimicrobial Agents and Chemotherapy* **46:**3292–3297.

Pommier Y, Marchand C & Neamati N (2000) Retroviral integrase inhibitors year 2000: update and perspectives. *Antiviral Research* **47:**139–148.

Ross WE, Glaubiger D & Kohn KW (1979) Qualitative and quantitative aspects of intercalator-induced DNA strand breaks. *Biochimica et Biophyssica Acta* **562:**41–50.

Ruscetti FW (1985) Immunopathology associated with human lymphotropic retroviruses. *Survey and Synthesis of Pathology Research* **4:**216–226.

Schauer M & Billich A (1992) The N-terminal region of HIV-1 integrase is required for integration activity, but not for DNA-binding. *Biochemical and Biophysical Research Communications* **185:**874–880.

Sunthitikawinsakul A, Kongkathip N, Kongkathip B, Phonnakhu S, Daly JW, Spande TF, Nimit Y & Rochanaruangrai S (2003) Coumarins and carbazoles from *Clausena excavata* exhibited antimycobacterial and antifungal activities. *Planta Medica* **69:**155–157.

Tamaoki T, Nomoto H, Takahashi I, Kato Y, Morimoto M & Tomita F (1986) Staurosporine, a potent inhibitor of phospholipid/Ca^{++} dependent protein kinase. *Biochemical and Biophysical Research Communications* **135:**397–402.

Tronchet JM & Seman M (2003) Non-nucleoside inhibitors of HIV-1 reverse transcriptase: from the biology of reverse transcription to molecular design. *Current Topics in Medicinal Chemistry* **3:**1496–1511.

Wilson WD & Jones RL (1982) Interaction of actinomycin D, ethidium, quinacrine, daunorubicin, and tetralysine with DNA: 31P NMR chemical shift and relaxation investigation. *Nucleic Acids Research* **10:**1399–1410.

Woerner AM & Marcus-Sekura CJ (1993) Characterization of a DNA binding domain in the C-terminus of HIV-1 integrase by deletion mutagenesis. *Nucleic Acids Research* **21:**3507–3511.

Received 22 August 2005, accepted 27 September 2005

JOURNAL OF VIROLOGY, Apr. 2005, p. 4720–4729
0022-538X/05/$08.00 0 doi:10.1128/JVI.79.8.4720–4729.2005

Vol. 79, No. 8

Role of the Specific Amino Acid Sequence of the Membrane-Spanning Domain of Human Immunodeficiency Virus Type 1 in Membrane Fusion

Kosuke Miyauchi,[1] Jun Komano,[1] Yoshiyuki Yokomaku,[2] Wataru Sugiura,[3] Naoki Yamamoto,[1,3] and Zene Matsuda[1]*

Laboratory of Virology and Pathogenesis[1] and Therapeutic Research and Clinical Science Group,[3] AIDS Research Center, National Institute of Infectious Diseases, Tokyo, and Division of Control and Treatment of Infectious Diseases, Chiba University Hospital, Chiba,[2] Japan

Received 16 July 2004/Accepted 6 December 2004

Fusion between cell and virus membranes mediated by gp41 initiates the life cycle of human immunodeficiency virus type 1. In contrast to the many studies that have elucidated the structure-function relationship of the ectodomain, the study of the membrane-spanning domain (MSD) has been rather limited. In particular, the role that the MSD's specific amino acid sequences may have in membrane fusion as well as other gp41 functions is not well understood. The MSD of gp41 contains well-conserved glycine residues that form the GXXXG motif (G, glycine; X, other amino acid residues), a motif often found at the helix-helix interface of membrane spanning -helices. Here we examined the role that the specific amino acid sequence of the gp41 MSD has in gp41 function, particularly in membrane fusion, by making two types of MSD mutants: (i) glycine substitution mutants in which glycine residues of the MSD were mutated to alanine or leucine residues, and (ii) replacement mutants in which the entire MSD was replaced with one derived from glycophorin A or from vesicular stomatitis virus G. The substitution of glycines did not affect gp41 function. MSD-replacement mutants, however, showed severely impaired fusion activity. The assay using the Env expression vector revealed defects in membrane fusion after CD4 binding steps in the MSD-replacement mutants. In addition, the change in Env processing was noted for MSD-replacement mutants. These results suggest that the MSD of gp41 has a relatively wide but not unlimited tolerance for mutations and plays a critical role in membrane fusion as well as in other steps of Env biogenesis.

The envelope glycoprotein (Env) of human immunodeficiency virus type 1 (HIV-1) plays a critical role in the entry process in the viral life cycle. Env is synthesized as a precursor, gp160, and then processed into a heterodimer consisting of gp120 and gp41. Interaction of gp120 with CD4 and chemokine receptors triggers the membrane fusion process.

The gp41 is believed to play a central role in the fusion process during postreceptor binding. It is divided into three subunits or domains: the extracellular, membrane-spanning, and cytoplasmic domains. The contribution of the extracellular domain to membrane fusion has been well documented. It contains conserved heptad repeats preceded by the fusion peptide and is thought to undergo conformational changes during membrane fusion to form a trimeric coiled-coil, commonly observed in the envelope proteins of viruses such as the influenza virus, the Moloney murine leukemia virus, and the Ebola virus (4–6, 11, 20, 37, 43, 44).

The cytoplasmic domain is relatively long compared with those of other simple animal retroviral envelope proteins and bears two well-conserved amphipathic helices called LLP1 and LLP2 (10, 25, 40). The cytoplasmic domain is important to intracellular trafficking as well as to the efficient incorporation of Env onto the budding viral particle (9, 32, 46). The cytoplasmic domain may affect fusion activity of Env (13, 27).

The membrane-spanning domain (MSD) of gp41 anchors Env on the lipid bilayer, and its amino acid sequences are highly conserved among independent isolates of HIV-1. Several studies have indicated that the MSD is involved in membrane fusion—the glycosylphosphatidylinositol-anchored Env of HIV-1, which lacks the MSD and the cytoplasmic domain, could not induce syncytia (35, 42). However, whether specific amino acid sequences in the MSD are required for its function in HIV-1 replication remains controversial. For example, the previous study showed that substituting a leucine residue for the conserved arginine residue within the MSD resulted in a replication-incompetent virus (31). Substituting isoleucine for the same arginine residue, however, did not affect gp41 function (42). Furthermore, fusion activity was retained in a mutant in which the entire MSD and cytoplasmic domain were replaced with those of CD4 (41). Wilk et al. have reported a replication-competent recombinant HIV-1 in which a CD22 MSD replaced the gp41 MSD (45). Because there is no apparent sequence homology among the MSDs of gp41, CD4, and CD22, these results suggest that gp41 function may not require a specific sequence in the MSD or, alternatively, that some as-yet-undetermined characteristic of CD4 and CD22 MSDs might compensate for the naturally occurring sequence. One feature common to the MSDs of gp41, CD4, and CD22 is the presence of several glycine residues (Fig. 1A). A glycine residue is not a rarity in the MSDs of membrane proteins (8, 39).

* Corresponding author. Mailing address: Laboratory of Virology and Pathogenesis, AIDS Research Center, National Institute of Infectious Diseases, 4-7-1 Gakuen Musashimurayama, Tokyo 208-0011, Japan. Phone: 81-42-561-0771-335. Fax: 81-42-562-7875. E-mail: zmatsuda@nih.go.jp.

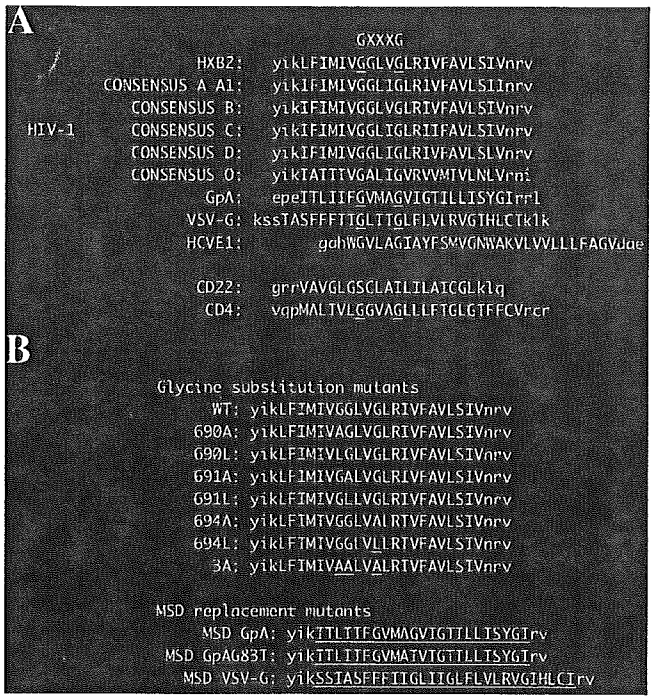

FIG. 1. Amino acid sequences of the MSD of HIV-1 isolates and several membrane proteins. (A) Amino acid sequences of the predicted MSD of HXB2, HIV-1 isolates, and several membrane proteins are shown. The sequence of HIV-1 isolates was according to HIV Sequence Compendium 2001 (17). The MSDs of CD4 and CD22 that could replace the MSD of gp41 without affecting gp41's function are also shown (41, 45). The capital letters indicate the amino acid sequences within the predicted MSD. The small letters indicate the amino acid sequences surrounding the MSD. Glycine residues in the GXXXG motif are underlined. (B) Amino acid sequences of MSD mutants. The mutated portions are underlined.

With respect to several viral membrane proteins, glycine residues are more often found in the MSDs of envelope proteins than in the MSDs of nonenvelope proteins (8). Although the importance of glycine residues in Env-mediated membrane fusion has been studied with viruses such as vesicular stomatitis virus (VSV) and the influenza virus (8, 23), the role of glycine residues in the MSD of gp41 has not been investigated.

In the gp41 MSD of HIV-1, the glycine residues form the GXXXG motif (G, glycine; X, other amino acid residues). This motif is often observed in transmembrane -helices and is believed to stabilize helix-helix interactions of membrane proteins (12, 34). In the case of glycophorin A (GpA) MSD, this motif is critical for homodimerization (26). A recent study showed that the transmembrane domains of hepatitis C virus E1 and E2 envelope glycoproteins are required in heterodimerization and that E1 also has the GXXXG motif in its MSD (29). The above-mentioned CD4 also contains the GXXXG motif. Thus, the maintenance of fusion activity in gp41 mutants having MSDs that were replaced with those of CD4 or CD22 might depend on the presence of glycine residues in the CD4 and CD22 MSDs (41, 45). To investigate whether the specific amino acid sequence in the MSD of gp41 is required for fusion activity, we mutated glycine residues or replaced the entire MSD of gp41 with heterologous MSDs and analyzed the effect that these mutations had on gp41 function. We found that the latter heterologous replacement enhanced the processing of gp160. The fusion activity of gp41 was severely impaired. Our analysis of the membrane fusion process of these mutants revealed that the defects are manifested in the postreceptor binding steps preceding lipid mixing and possibly in the steps after the initial pore formation.

MATERIALS AND METHODS

Construction of plasmids. The 1.2-kb NheI-BamHI fragment covering the *env* portion of the modified HXB2, HXB2RU3 N (*vpr* , *vpu* , *nef* , and one NheI site within the vector were deleted), was subcloned into pGEM7zf( ) (Promega, Madison, Wis.) as a target for mutagenesis. To generate each glycine substitution (Gly^{sub}) mutant, site-directed mutagenesis was performed using a QuikChange site-directed mutagenesis kit (Stratagene, La Jolla, Calif.) with complementary oligonucleotide pairs (for 690A, CATAATGATAGTAGCAGGCTTGGT AGGT and ACCTACCAAGCCTGCTACTATCATTATG; for 690L, CATAA TGATAGTACTAGGCTTGGTAGGT and ACCTACCAAGCCTAGTACTAT CATTATG; for 691A, ATGATAGTAGGAGCCTTGGTAGGTTTA and TAA ACCTACCAAGGCTCCTACTATCAT; for 691L, ATGATAGTAGGACTCT TGGTAGGTTTA and TAAACCTACCAAGAGTCCTACTATCAT; for 694A, AGGAGGCTTGGTAGCTTTAAGAATAGTTTTTG and CAAAAACTATT CTTAAAGCTACCAAGCCTCCT; and for 694L, AGGAGGCTTGGTACTTT TAAGAATAGTTTTTG and CAAAAACTATTCTTAAAAGTACCAAGCCT CCT), generating the substitution of an alanine or a leucine residue for a glycine residue. The PCR was performed using Pfu turbo (Stratagene). The 3A mutant was created by site-directed mutagenesis using a complementary oligonucleotide pair (CATAATGATAGTAGCCGCCTTGGTAGCCTTAAGAATAGTTTTTG and CAAAAACTATTCTTAAGGCTACCAAGGCGGCTACTATCATTATG).

To generate the MSD-replacement mutants, megaprimers that were produced by PCR that targeted the MSD portion of VSV-G or GpA as a template were used as mutagenesis oligonucleotides (for MSD GpA, CAAATTGGCTGTGG TATATAAAAATCACCCTGATCATC and GAATATCCCTGCCTAACTCT GATGCCGTAGCTGAT; for MSD VSV-G, CAAATTGGCTGTGGTATATA AAAAGCTCTATTGCCTC and GAATATCCCTGCCTAACTCTAATGCAA AGATGGATAC). MSD GpAG83I was produced by site-directed mutagenesis using a subclone of MSD GpA as a template with a primer set (CATCTTCGG CGTGATGGCCATCGTGATCGGCACCATCCTG and CAGGATGGTGCC GATCACGATGGCCATCACGCCGAAGATG). Following mutagenesis, the 1.2-kb NheI-BamHI fragments were sequenced and cloned back into the pSP65HXB2RU3 N plasmid. After the cloning back, the entire NheI-BamHI portion together with the junction was verified by sequencing.

An Env expression vector, pElucEnv, was used to express *env* genes in this study. Although the details of its construction will be described elsewhere, it is a derivative of pSP65HXB2RU3 N and lacks the *gag* and *pol* portions of the provirus. The *rev* function was provided by *rev* cDNA cloned into the *nef* region. The original *rev* gene was inactivated by mutating its initiation codon. A BsiWI site was introduced near the initiation codon of the original *rev* gene by this mutagenesis. Because this vector contains an enhanced green fluorescent protein (EGFP)-firefly luciferase expression module outside the provirus, the transfected cells fluoresce green, allowing us to estimate transfection efficiency by measuring firefly luciferase activity. To generate each Env expression vector, the NheI-BamHI fragment of the pSP65HXB2RU3 N wild type (WT), MSD GpA, MSD GpAG83I, or MSD VSV-G was cloned into pElucEnv. As a negative control, pElucEnv EnvKO was produced. The *env* gene of pElucEnv EnvKO has a stop codon after its 25th codon. The 2.7-kb SalI-BamHI fragment covering the *env* portion of the pElucEnv WT was subcloned into pGEM3zf( ) (Promega) as a target for the mutagenesis. The site-directed mutagenesis used to create the stop codon was performed with a specific primer set (CTCCTTGGGATGTTGTAG ATCTGTAGTCTACA and TGTAGCACTACAGATCTACAACATCCCAAG GAG). The BsiWI-BamHI fragment of the subclone was sequenced and cloned back into pElucEnv WT.

A reporter vector, pTM3hRL, which has a reporter gene, renilla luciferase, under the control of the T7 promoter, was generated from the pTM3luci vector (1) by replacing the firefly luciferase gene with the humanized renilla luciferase gene. The renilla luciferase gene was amplified from phRL-CMV vector (Promega) by PCR with a primer set (CGACTCACTATAGGCTAGCC and GCT CGAGGCGGCCGCTCTAGAATTAC), cloned into pCR4Blunt-TOPO (Invitrogen, Carlsbad, Calif.), and sequenced before cloning. To generate the T7 RNA-polymerase (T7 RNApol) expression vector, pCMMP T7RNApoliresGFP, the gene encoding T7 RNA polymerase, was PCR amplified from pVR-T7-1 (1)

and cloned into the pCMMP retrovirus vector (30). In this vector, the T7 RNApol gene is followed by an internal ribosome entry site and a GFP gene.

Cells and antibodies. COS7 cells, 293 cells, and MAGI cells were grown in Dulbecco's modified essential medium (DMEM; Sigma, St. Louis, Mo.) supplemented with 10% fetal bovine serum (FBS) (HyClone Laboratories, Logan, Utah) and penicillin-streptomycin (Gibco-BRL, Rockville, Md.). MAGI cells were grown in DMEM supplemented with 10% FBS, penicillin-streptomycin, Geneticine (0.2 mg/ml), and hygromycin B (0.1 mg/ml) (16). Jurkat cells and H9 cells were grown in RPMI 1640 (Sigma) supplemented with 10% FBS and penicillin-streptomycin. Cells were kept under conditions of 5% CO_2 in a humidified incubator. OKT4 is an anti-CD4 monoclonal antibody and was obtained from Ortho Diagnostic System (Raritan, N.J.). Anti-gp120 polydonal antibody was obtained from Fitzgerald Industries International, Inc. (Concord, Mass.). The purified anti-gp120 monoclonal antibody prepared from hybridoma 902 was kindly provided by Y. Yokota of the National Institute of Infectious Diseases, Tokyo, Japan. Hybridoma 902 was obtained from Bruce Chesebro through the AIDS Research and Reference Reagent Program, Division of AIDS, National Institute of Allergy and Infectious Diseases, National Institutes of Health (7, 33). 293CD4 cells were isolated from 293 cells that had been transfected with pMACS 4-IRESII (Miltenyi Biotec GmbH, Bergisch Gladbach, Germany) by use of a MACSelect4.2 system (Miltenyi Biotec GmbH). Serum from a patient infected with HIV-1 was kindly provided by T. H. Lee of Harvard School of Public Health, Boston, Mass.

Protein analysis. The WT and mutant HXB2RU3 N constructs were transfected into COS7 cells by the use of Gene Pulsar II (Bio-Rad, Hercules, Calif.). In brief, COS7 cells were suspended in serum-free DMEM and electroporated with 4 g of proviral DNA at a setting of 250 kV and 950 F. At 72 h after transfection, cell and virus lysates were prepared for protein analysis. Transfected COS7 cells were collected by scraping and were centrifuged (Allegra 6KR system; Beckman Coulter, Fullerton, Calif.) at 2,000 *g* for 10 min. The cell pellets were dissolved in radioimmunoprecipitation assay lysis buffer (0.05 M Tris-Cl [pH 7.2] including 0.15 M NaCl, 1% Triton X-100, 1% sodium deoxycholate, and 0.1% sodium dodecyl sulfate [SDS]) and centrifuged (Himac CS 120fx system; Hitachi, Tokyo, Japan) at 314,000 *g* for 45 min at 4°C. The supernatants were subjected to SDS-polyacrylamide gel electrophoresis (PAGE). To analyze viral proteins, the supernatants from culture media were spun (Allegra 6KR system) (2,000 *g* for 20 min) to clear cell debris, filtered through 0.45- m-pore-size filters (Millipore, Bedford, Mass.), and then centrifuged (SW28 rotor; Beckman Coulter) at 4°C for 1.5 h on 3 ml of a 20% sucrose cushion at 113,000 *g*. Virus pellets were dissolved in radioimmunoprecipitation assay lysis buffer for protein analysis by SDS-PAGE. Cell and virus lysates were run on an SDS polyacrylamide gel (DRC, Tokyo, Japan) (7.5 to 15% gradient), and proteins were blotted onto Immobilon-P (Millipore) by passive transfer as described previously (21). The immunoblotting procedure was as follows. Before addition of the serum or monoclonal antibodies, the membranes were blocked with 3% bovine serum albumin (Sigma) dissolved in 0.2% Tween 20–PBS at room temperature for 30 min. Enhanced chemiluminescence (Roche Molecular Biochemicals, Mannheim, Germany) and a lumi-imager (Roche) were used to detect the bands after probing with the patient serum or with anti-gp120 polyclonal antibody. Anti-human- and anti-goat-sheep immunoglobulin G-biotin conjugates and streptavidin-horseradish peroxidase were purchased from Amersham Biosciences UK Limited (Buckinghamshire, United Kingdom).

MAGI cell assay. MAGI cells were cultured in a 96-well plate for 48 h and then transfected with 0.25 g of proviral DNA by FuGene6 (Roche Molecular Biochemicals). At 48 after transfection, the transfected MAGI cells were fixed using PBS containing 0.5% glutaraldehyde and were stained for -galactosidase as described previously (16). The nuclei in multinucleated cells were counted. Five randomly selected fields were evaluated for each mutant.

Infection study. For the infection study, the virus seed was prepared by transfecting 1 g of the proviral DNA into 10^6 of COS7 cells by FuGene6. At 72 h after transfection, the culture supernatant was filtered through 0.45- m-pore-size filters (Millipore) and the p24 amount was determined using a p24 enzyme-linked immunosorbent assay (ELISA). Jurkat cells were infected with each virus adjusted by the p24 amount (10 ng of p24 per 10^6 cells to be infected). The infection was monitored by measuring the p24 amount of the culture supernatant at the indicated time point after infection. A p24 ELISA was performed using a p24 RETRO-TEK ELISA kit (ZeptoMetrix, Buffalo, N.Y.).

Flow cytometry. At 48 after transfection by FuGene6, the COS7 cells that had been transfected with each Env expression vector (pElucEnv WT, MSD GpA, MSD GpAG83I, MSD VSV-G, or EnvKO) were stained with the 902 monoclonal antibody for 1 h at 4°C (10 g/ml in PBS with 2% FBS), incubated with biotin-XX goat anti-mouse immunoglobulin G (Molecular Probes, Eugene, Oreg.) for 30 min at 4°C, and then treated with streptavidin Alexa Fluor 555 (Molecular Probes) for 30 min at 4°C and finally fixed with 1% paraformaldehyde in PBS. Cells were suspended in PBS with 2% FBS and analyzed with Becton Dickinson FACSCalibur and CellQuest software (BD Biosciences Immunocytometry Systems, San Jose, Calif.). A double gate was defined by forward versus side scatter and by the amount of GFP (FL-1). A total of 10,000 events within this gate were collected for analysis.

CD4-binding assay. To evaluate the CD4-binding capacity of each MSD-mutant Env, cell lysates prepared from the COS7 cells transfected with each Env expression vector (pElucEnv WT, MSD GpA, MSD GpAG83I, or MSD VSV-G) and a CD4 expression vector by FuGene6 were prepared. At 72 h after transfection, the transfected COS7 cells were suspended in 250 l of a binding buffer, 0.5% Triton X-100 in PBS, supplied with the Complete protease-inhibitor cocktail (Roche Molecular Biochemicals). Aliquots of 50 l from each lysate were mixed together, and 2 l of OKT-4 and 5 l of protein G Magnetic Beads (New England BioLabs, Beverly, Mass.) were added. After a 1-h incubation at 4°C, the beads were washed twice with 200 l of binding buffer and subjected to SDS-PAGE. The gp120 was detected using an immunoblotting analysis (see above).

Dye-transfer assay. The COS7 cells were transfected with each Env expression vector (pElucEnv WT, MSD GpA, MSD GpAG83I, EnvKO, or MSD VSV-G) by FuGene6 and cocultured with H9 cells at 48 h after transfection. H9 cells used for this assay were loaded with CellTracker CM-DiI (at a final concentration of 10 M) and Calcein blue, AM (Molecular Probes) (at a final concentration of 40 M), precultured for 3 h, and then washed with culture medium. At 2 h after coculture, the cells were fixed with 4% paraformaldehyde–PBS and analyzed using a Zeiss LSM510META microscope. Cells showing green, red, or blue fluorescence were counted in each of five randomly selected fields at magnification of 200.

T7 RNApol transfer assay. The COS7 cells were transfected with each Env expression vector (pElucEnv WT, MSD GpA, MSD GpAG83I, MSD VSV-G, or EnvKO) together with pTM3hRL (see above) by the use of FuGene6. At 48 after transfection, the transfected COS7 cells were cocultured with the 293CD4 cells that had been transfected with the T7 RNApol expression vector, pCMMP T7RNApolresGFP (the ratio of cells was 1:1). At 12 h after coculture, the cells were lysed and the firefly luciferase activities, derived from the Env expression vector, and renilla luciferase activities, activated by the T7 RNApol transferred from 293CD4 cells through the generated fusion pores, were determined using a Dual-Glo luciferase reporter assay system (Promega).

RESULTS

Gly^{sub} mutations did not affect the fusion activity of gp41 in MAGI cells. The amino acid sequences of the predicted MSD of HXB2, the consensus sequences of HIV-1 subtypes, and sequences of certain other membrane proteins are shown in Fig. 1A. Although the MSDs of CD22 and CD4 could replace the MSD of gp41 without affecting its function (41, 45), the lengths of the predicted MSDs differ and there is no apparent sequence homology among them except for the presence of several glycine residues. The amino acid sequence of the MSD of gp41 is well conserved among different clades, and it contains the GXXXG motif. Except for the MSD in CD22, all MSDs listed contain the GXXXG motif. To evaluate the relative contributions that the three glycine residues in the gp41 MSD made to fusion activity, each glycine residue was changed to an alanine or a leucine residue. Additionally, all three glycine residues were changed to alanine residues in the 3A mutant. The amino acid sequences and nomenclatures of Gly^{sub} mutants are shown in Fig. 1B. Alanine and leucine residues were chosen because they are commonly found in the transmembrane region of membrane proteins (39). In a previous study, substituting alanine or leucine residues for glycine residues in VSV-G produced membrane-fusion-incompetent proteins (8).

The protein profile of Gly^{sub} mutants was examined by immunoblotting analysis of both cell and virus lysates derived from COS7 cells transfected with the proviral DNAs. Similar

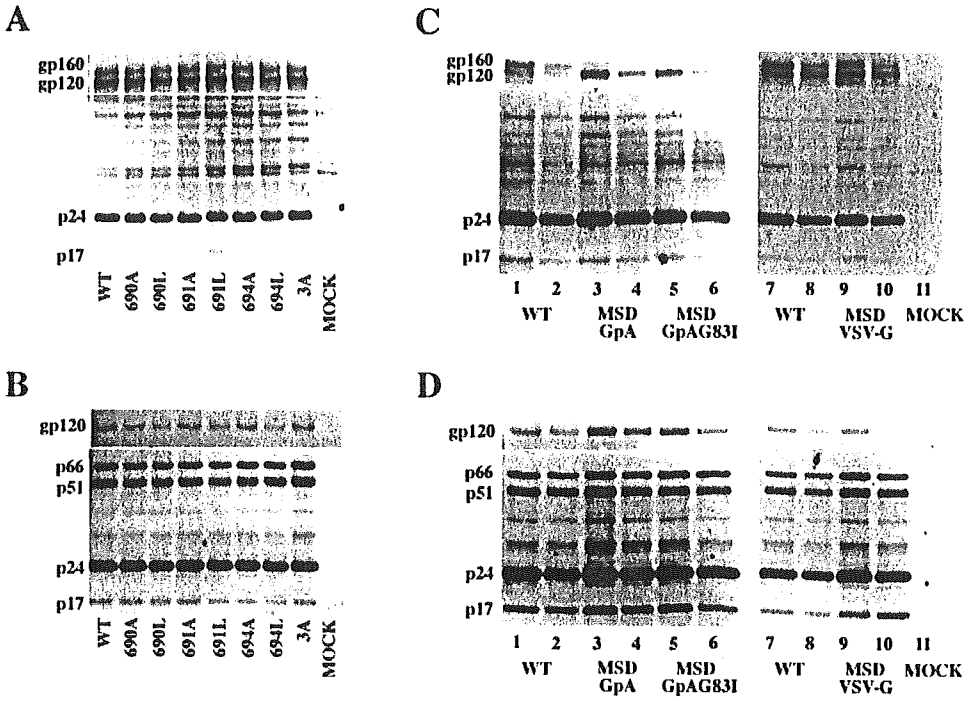

FIG. 2. Protein profiles of cell and virus lysates of the WT and mutants. The cell and virus lysates for glycine substitution (A and B) and MSD replacement mutants (C and D) were prepared from COS7 transfected with proviral DNA. The Env proteins (gp160, gp120) were detected with anti-gp120 polyclonal antibody. Gag (p24, p17) and Pol (p66, p51) were detected using serum from an individual infected with HIV-1. The name of the provirus DNA is indicated below, and the bands corresponding to gp160, gp120, p66, p51, p24, and p17 are shown by arrows. (C and D) For MSD replacement mutants, two different amounts of lysates were loaded for each mutant. The second lane of each sample received an amount of the lysate that was half of the amount used for the preceding lane.

protein profiles were observed for all Gly^{sub} mutants and the WT in both cell and virus lysates (Fig. 2A and B). For all Gly^{sub} mutants, both gp160 and gp120 were detected in cell lysates and gp120 was detected in virus lysates. We did not observe prominent changes in Env processing, as in the case of the MSD replacement (MSD^{rep}) mutants (see below). In virus lysates, similar levels of Env relative to virus Gag/Pol products (p17, p24, p51, and p66) were detected in each sample (Fig. 2B). These data suggested that all the Env mutants were expressed, processed, transported to the plasma membrane, and incorporated onto the virions. Fusion activities of the Gly^{sub} mutants were evaluated by a MAGI cell assay using an arbitrary fusion index that reflects both the number of syncytia and the number of nuclei within a syncytium. As shown in Fig. 3, the fusion index of all Gly^{sub} mutants was comparable with that of the WT. Notably, the fusion activity of the 3A mutant was also well maintained (Fig. 3). These data suggested that glycine residues in the MSD of gp41 were not necessary for membrane fusion in MAGI cells.

Gly^{sub} mutants retained the replication capacity in Jurkat cells. We next evaluated the effect of glycine substitution on viral replication in T-cell lines. Viruses collected from the culture supernatants of COS7 cells transfected with the proviral DNAs were used to infect Jurkat or H9 cells. Replication of mutant viruses was monitored by measuring the amount of p24 released into the culture medium. A representative result is shown in Fig. 4. All Gly^{sub} mutants were replication competent and showed replication kinetics similar to those of the WT virus in Jurkat cells. Similar results were observed in H9 cells (data not shown). These results were consistent with the results of fusion assay in MAGI cells (Fig. 3) and suggested that the contribution of glycine residues in MSD to the life cycle of HIV-1 was relatively small.

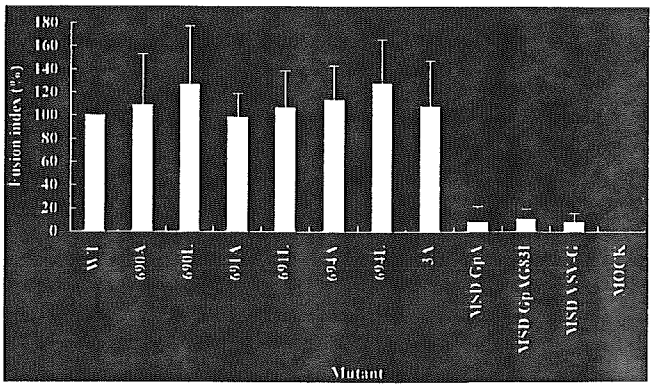

FIG. 3. Relative fusion activity of MSD mutants in MAGI cell assay. Fusion activity of the WT and MSD mutants was expressed using a fusion index (fusion index $2x$ y, where x is the number of multinucleated cells [number of nuclei 5 in five visual fields] and y is the number of multinucleated cells [number of nuclei 5 in five visual fields]). The fusion index was defined to reflect the number of nuclei in multinucleated cells. Fusion activities for each mutant are shown after normalization to that of the WT (the WT activity was set at 100%). Similar results were obtained in three independent experiments.

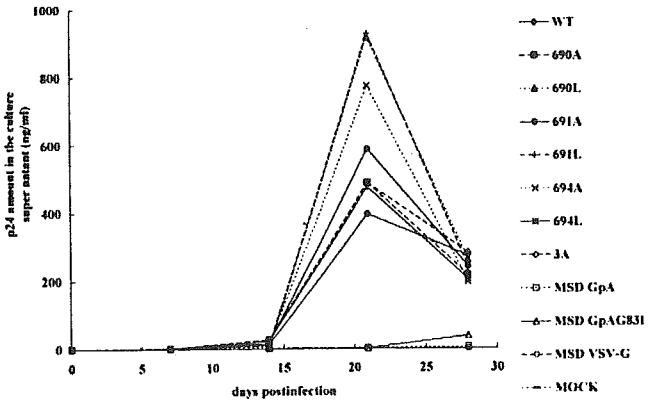

FIG. 4. Replication profiles of the WT and MSD mutants in Jurkat cells. Viral stocks of the WT and each mutant were prepared from culture supernatant of COS7 cells transfected with proviral DNA, and Jurkat cells were infected with each virus adjusted by the amount of p24. Replication was monitored by measuring the amount of p24 in the culture supernatant at specific time points following infection. A representative result of three independent experiments is shown.

The protein profile of MSD^{rep} mutants was altered. Our data for Gly^{sub} mutants suggested that the MSD of gp41 might have a rather high tolerance for mutation. To examine the extent to which the gp41 MSD tolerated more drastic changes in amino acid sequences, the entire MSD of gp41 was replaced with that of VSV-G, GpA, or GpAG83I. The sequence of each MSD is shown in Fig. 1B. Both GpA and VSV-G contain the GXXXG motif within their MSDs. The former takes a dimer, and the latter forms a trimer. The GpAG83I is a GpA mutant that lacks homodimerization activity owing to the substitution of the 83rd glycine residue (the numbering is according to the system used for GpA study) with an isoleucine residue. This GpAG83I was included to overcome the potential negative effect of the homodimerization activity of GpA (34).

The expression of viral gene products from MSD^{rep} mutants was examined by immunoblotting analysis using cell and virus lysates derived from COS7 cells transfected with the proviral DNAs. Two different amounts of each lysate type (cell and virus) were loaded for each construct to achieve semiquantitative evaluation of the band intensity. The second lane of each sample received an amount of the lysate that was half that of the preceding lane. In cell lysates, the reproducible change in the processing pattern of Env was noted for MSD^{rep} mutants. All MSD^{rep} mutants showed more signal for gp120 than for gp160 (Fig. 2C). This was most prominent in GpA and GpAG83I mutants, followed by the VSV-G mutant (Fig. 2C). The sum intensity of gp160/gp120 normalized by the p24 amount was approximately same for both MSD^{rep} mutants and the WT.

This semiquantitative analysis was also performed for virus lysates (Fig. 2D). In virus lysates, the intensity for gp120 relative to p24 was stronger for GpA and GpAG83I mutants (compare lane 1 with lane 4 or 5 in Fig. 2D). Compared with the WT, the VSV-G replacement mutant showed relatively more p24 for an approximately equivalent amount of gp120 (compare lanes 7 and 9 in Fig. 2D). This may indicate that the VSV-G mutant incorporated Env less efficiently than the WT or that Env was shed by the VSV-G mutant. Thus, there were some alterations in expression, processing, and transport to the plasma membrane and in the incorporation onto the virions in Env of MSD^{rep} mutants in the provirus context. Next we evaluated the function of Env of MSD^{rep} mutants.

Fusion activity of MSD^{rep} mutants was significantly decreased. The MAGI cell assay was used to examine the fusion activity of MSD^{rep} mutants. Compared with the WT, far fewer multinucleated cells were observed in MSD^{rep} mutants. Although syncytia were occasionally observed in an MSD^{rep} mutant, each syncytium observed contained fewer nuclei than any given syncytium observed in the WT. Thus, fusion indices of MSD^{rep} mutants were very low compared with those of the WT (Fig. 3). These observations suggested the presence of defects in the membrane fusion steps themselves, because changes in the expression level and the processing of Env in cell lysates (Fig. 2C) alone did not seem to be able to account for the observed severe defect in fusion. These defects were partially compensated for when we used a HeLa–CD4-derived cell line that had a higher level of CD4. In this cell line, the efficiency of syncytia formation and the number of nuclei in a syncytium were increased (data not shown). Consistent with the defect in fusion activity, MSD^{rep} mutants showed severely impaired replication capacity in Jurkat cells (Fig. 4) and in H9 cells (data not shown). We tried to determine the point at which membrane fusion ceased in MSD^{rep} mutants by using the Env expression vector.

The cell surface expression and CD4-binding capacity of Env for MSD^{rep} mutants were similar to those for WT. We constructed the Env expression vectors to analyze the steps of membrane fusion processes of MSD^{rep} mutants (Fig. 5A). First, we examined the cell surface Env expression of MSD^{rep} mutants by transfecting each Env expression vector into COS7 cells and then performing a flow cytometric analysis using an anti-gp120 monoclonal antibody. As the transfected cells expressed GFP derived from the expression vector, cells were gated for GFP first. A representative result is shown in Fig. 5B. The fluorescence intensities of Env in MSD^{rep} mutants and the WT were nearly equal. The expression of Env was also verified by Western blotting analysis (data not shown).

Next, we tested the CD4-binding capacity of the Env of MSD^{rep} mutants, because mutations in MSDs potentially affect the conformation of Env. We immunoprecipitated CD4 by using anti-CD4 antibody from a mixture of cell lysates prepared from COS7 cells that had been transfected with either the CD4 expression vector or the Env expression vector. The gp120 that coimmunoprecipitated with the CD4 was detected using immunoblotting analysis. The gp120 coimmunoprecipitated at similar efficiencies in MSD^{rep} mutants and the WT (Fig. 5C). These data suggested that the MSD replacement did not affect the CD4-binding capacity of the mutated Envs. Thus, the membrane fusion defect of Envs of MSD^{rep} mutants was determined to be in the post-CD4-binding steps.

Examination of the hemifusion and fusion pore formation steps in MSD^{rep} mutants. We used the dye-transfer assay to examine whether Envs of MSD^{rep} mutants were able to induce lipid mixing and fusion pore formation between Env- and receptor-expressing cells. In this assay, the COS7 cells transfected with a recombinant Env expression vector bearing the EGFP-firefly luciferase hybrid gene (Fig. 5A) were cocultured with T cells whose cell membrane and cytoplasm were labeled

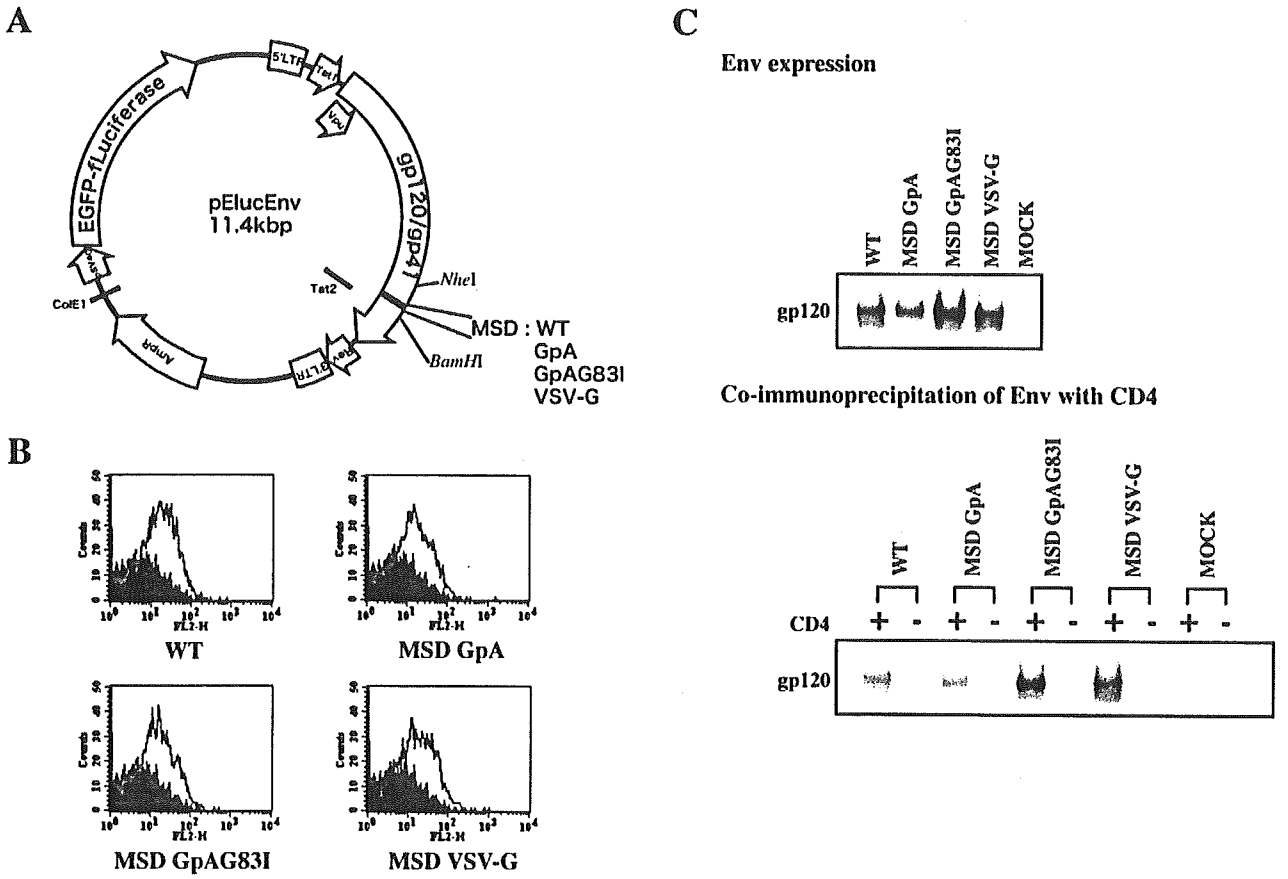

FIG. 5. Evaluation of the cell surface expression and the CD4-binding capacity of Env of MSD mutants. (A) The map of the Env expression vector pElucEnv. pElucEnv supports the expression of HIV-1 *env* (gp120/gp41) and the gene of the EGFP-firefly luciferase (EGFP-fLuciferase) hybrid protein from two separate promoters. The NheI-BamHI fragments of pSP65HXB2RU3 N WT, MSD GpA, MSD GpAG83I, or MSD VSV-G were cloned into pElucEnv. 5 LTR, 5 long terminal repeat of HIV-1; 3 LTR, 3 long terminal repeat of HIV-1. *tat*, *vpu*, and *rev* represent *tat*, *vpu*, and *rev* of HIV-1. AmpR, beta-lactamase; SV40, simian virus 40 late promoter; ColE1, ColE1 replication origin; NheI and BamHI, restriction sites used for cloning of the mutated *env*. (B) Cell surface expression of Env. COS7 cells were transfected with each pElucEnv construct and subjected to flow cytometric analysis as described in the Materials and Methods section. The signal for each Env is shown with a gray line. The filled area depicts the signal obtained for the control vector, EnvKO. (C) CD4-binding capacity of Env of MSD mutants. The cell lysates prepared from the COS7 cells that had been transfected with the pElucEnv construct or the CD4 expression vector were mixed together, and CD4 was immunoprecipitated using OKT-4. The amount of gp120 coimmunoprecipitated with CD4 was evaluated. The upper panel shows the expression level of each Env mutant. Coimmunoprecipitated gp120 was detected using anti-gp120 polyclonal antibodies (shown in the lower panel).

with CM-DiI (red) and Calcein blue, AM (blue), respectively. When the lipids from the two cells mix, a transfer of red dye should be observed. If fusion pores are formed, fused cells whose cytoplasm bears both blue and green fluorescence should appear. The results are shown in Fig. 6. At 2 h after coculture, cells having green, red, and blue fluorescence were observed in the WT (Fig. 6A). Similar cells were also observed in MSD^{rep} mutants but were fewer in number than those observed in the WT. We determined the frequency of lipid or cytoplasmic mixing 2 h after coculture by counting Env-expressing cells (green cells) whose membrane or cytoplasm was stained with CM-DiI or Calcein blue, AM, respectively. In MSD^{rep} mutants, many Env-expressing COS7 cells were surrounded by T cells and showed no evidence of dye transfer. The relative frequency of dye transfer was determined to be less than half that of the WT (Fig. 6B). In this assay, we did not observe significant discrepancies in the frequencies with which the two dyes were transferred; that is to say, cells arrested at the hemifusion stage were not detected. These data suggested that Env of MSD^{rep} mutants retained the capacity for fusion but at efficiencies that were much lower than those of the WT and that failed to produce large syncytia. The decrease in transfer of CM-DiI indicated that MSD^{rep} mutants had a defect that affected the fusion process prior to hemifusion. The smaller size of the syncytia observed in MSD^{rep} mutants may suggest the presence of other defects after hemifusion, possibly an enlargement of fusion pore.

We performed an additional quantitative assessment of fusion pore formation by the use of the T7 RNApol transfer assay. In this assay, COS7 cells were first transfected with an Env expression vector coupled with a reporter plasmid, pTM3hRL, which encodes T7 promoter-driven renilla luciferase, and then were cocultured with 293CD4 cells that had been transfected with a T7 RNApol expression plasmid. When the COS7 and 293CD4 cells fused, the T7 RNApol in the 293CD4 cells transferred into the COS7 cells and drove ex-

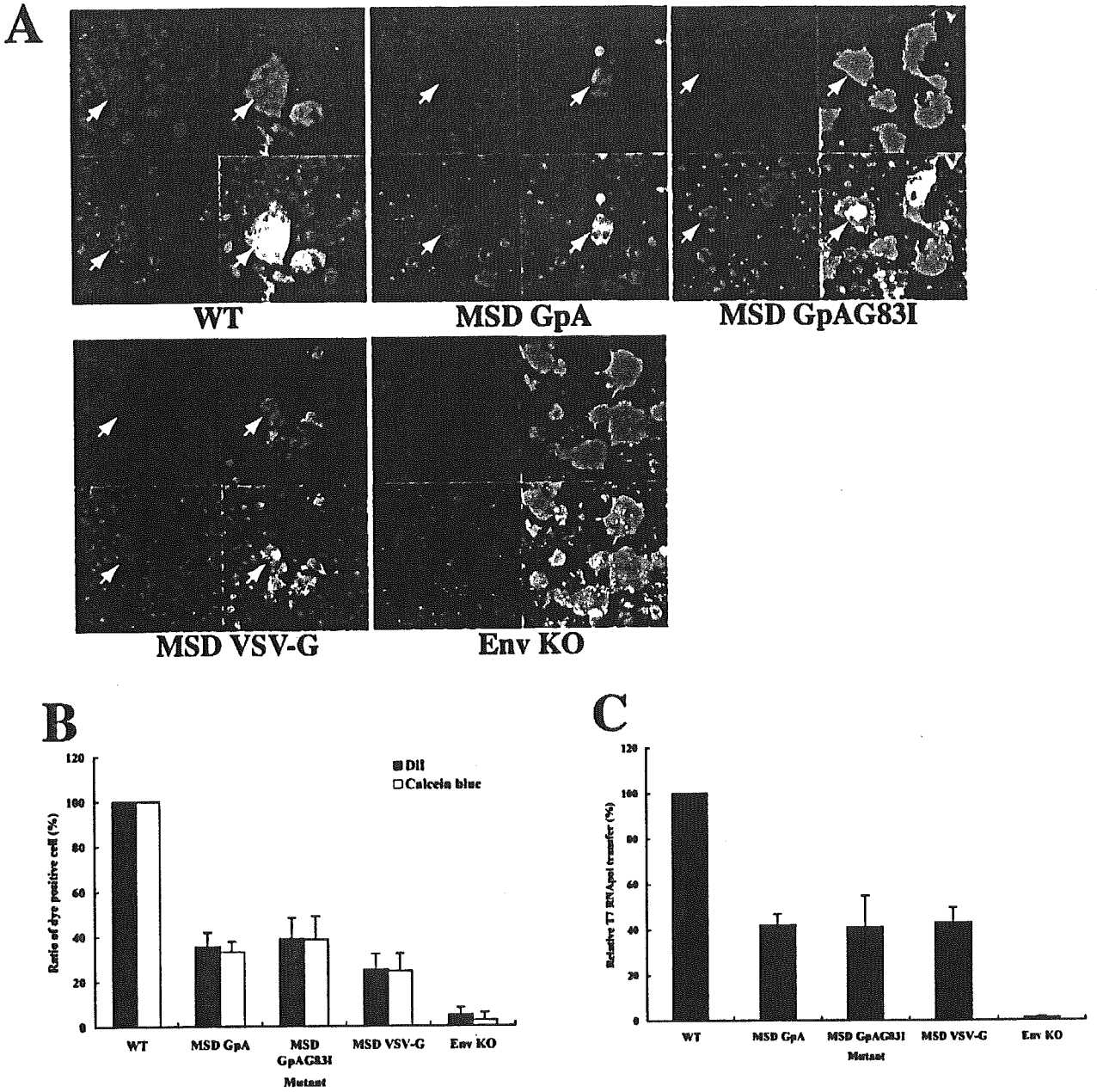

FIG. 6. Cell-cell fusion analysis. The results of a dye-transfer assay using a coculture system and COS and T cells are shown. The COS7 cells transiently transfected with each pElucEnv construct were cocultured with H9 cells that had been loaded with CellTracker CM-DiI (pseudo-red) and Calcein blue, AM (pseudo-blue). Pictures taken at 2 h after coculture are shown in panel A. Typical fused cells having green, red, or blue fluorescence are indicated by arrows. Original magnification, 200. (B) Relative dye-transfer frequencies of MSD^{rep} mutants. The number of Env-expressing cells (green cells) whose membranes or cytoplasms are labeled with CM-DiI (red) or Calcein blue, AM (blue), respectively, was counted in five, randomly selected fields. The value was established by setting WT at 100%. The averages of the results from four experiments are shown. (C) Results of T7 RNApol-transfer assay to determine fusion pore formation of MSD mutants. The COS7 cells were transfected with each pElucEnv construct and the T7 RNApol-responsive reporter plasmid, pTM3hRL. At 48 h after transfection, the transfected COS7 cells were cocultured with the 293CD4 cells that had been transfected with pCMMP T7RNApoliresGFP. At 12 h after coculture, the cells were lysed and firefly luciferase and renilla luciferase activity levels were measured. Pore formation efficiencies were calculated by comparing the induced renilla luciferase activity to the firefly luciferase activity. A representative result of four independent experiments is shown.

pression of renilla luciferase. At 12 h after coculture, renilla luciferase activities were measured. The value was normalized according to the efficiency of transfection measured by firefly luciferase activities derived from the Env expression vector. Representative results are shown in Fig. 6C. Normalized renilla luciferase activities of MSD GpA, MSD GpAG83I, MSD VSV-G, and EnvKO were, respectively, 42, 41, 43, and 1.3% of that of the WT. Thus, the transfer of T7 RNApol observed for cells that were expressing MSD^{rep} Env was less efficient than that of the WT, a finding consistent with that from the dye-

transfer assay. We also tested a cleavage site mutant of Env (R511S) (3), which cannot produce an active fusion peptide and is unable to induce membrane fusion in this assay. The value was 2.6%. Therefore, the value obtained for MSD^{rep} mutants should reflect the efficiency of de novo pore formation. The value of around 40% of that of the WT obtained for MSD^{rep} mutants may appear high compared with the severe defects in the MAGI assay (Fig. 3) and replication assay (Fig. 4). This could be the result of differences in the two assay systems or it might suggest the presence of additional defects in membrane fusion in MSD^{rep} mutants.

DISCUSSION

The involvement of the MSD in membrane fusion has been studied for several different viruses, including HIV-1 (8, 14, 15, 22, 23, 28, 35, 36, 38, 42). However, the precise molecular mechanism of Env-mediated membrane fusion is not known, and the role of MSD, including whether the specific amino acid sequences in MSD are required for the membrane fusion process, is not well understood. Examination of the presently available HIV-1 sequence database reveals a high conservation of MSD sequences for gp41 (17). There also are several well-conserved glycine residues that form the GXXXG motif, a motif found in the helix-helix interface of many membrane-spanning -helices (24, 26, 29). Interestingly, the MSDs of CD4 and CD22, which can replace the MSD of gp41 without affecting its fusion activity, also contain several glycine residues. Building from these findings, we investigated whether the specific sequence of the gp41 MSD is required for competent membrane fusion. We did this by mutating the conserved glycine residues in the gp41 MSD to alanine or leucine residues. A similar mutation of glycine introduced into VSV-G has a detrimental effect on membrane fusion (8). Contrary to our expectations, mutation of glycine residues resulted in fusion-competent gp41 (Fig. 3). Even replacing all three glycine residues in gp41 MSD with alanine residues did not affect fusion activity (Fig. 3). This suggests that, in vitro, the gp41 MSD has a rather high tolerance for mutation. The conservation of glycine residues observed in field isolates may indicate that HIV-1 requires glycine residues for in vivo infection of cells whose properties are different from those seen with in vitro T-cell lines. This may also imply that the potential mechanisms involved in membrane fusion differ for gp41 and VSV-G. It may be that the contribution of the proposed kink in the MSD, induced by the presence of a glycine residue during VSV-G-mediated membrane fusion, is not as critical to the membrane fusion process in gp41 as it is for the same process in VSV-G (8). To further verify the role of GXXXG motif for a potential helix-helix association motif, future analyses may require simultaneous substitution of all glycines with other bulky amino acid residues.

Proceeding on the basis of our results obtained with Gly^{sub} mutants and previous reports of replication-competent HIV-1 having heterologous MSD in place of the natural gp41 MSD, we next replaced the entire gp41 MSD with MSDs of heterologous membrane proteins (GpA or VSV-G). Membrane fusion activity was severely impaired in both the GpA and VSV-G replacement mutants (Fig. 3). Because GpA is known to form a dimer through the GXXXG motif, the dimerization activity may interfere with the proper trimerization of gp41 and cause the observed defect. However, the observed defect was not rescued by introducing a G83I mutation within the MSD of GpA (Fig. 3), a mutation that has been shown to knock out the dimerization ability (34). Therefore, the defect cannot be explained simply by noting that replacing the MSD interfered with gp41's proper trimerization. A similar defect in membrane fusion observed in our VSV-G–replacement mutant may further support this argument, because VSV-G, like gp41, is reported to form a trimer. At this time, however, we cannot completely rule out the potential defect in proper trimerization of Env in the MSD replacement mutants.

It is worth mentioning that we observed more gp120 than gp160 reproducibly in MSD^{rep} mutants, especially for GpA-replacement mutants in the transfected cells. This may suggest that there are some subtle conformational changes in Env for the GpA-replacement mutants that allow for more efficient processing by the furin-like protease. It also suggests that the mutation may alter the length of time needed for the mutant envelope proteins to travel through the *trans* Golgi network. These possibilities are consistent with a hypothesis that mutation within the MSD may affect the intracellular trafficking of the envelope protein. We cannot rule out this hypothesis.

In the provirus context, a smaller amount of Env was detected in virus lysates for VSV-G replacement mutant (Fig. 2D). This defect, in addition to the defect in fusion, may contribute to the VSV-G replacement mutant's inability to replicate (Fig. 4). The mechanism of this defect is not known at present. The mutation within the MSD, however, may affect the structure of gp41 and that, in turn, may result in a less efficient interaction between Gag and Env during assembly or a less stable association between gp41 and gp120 in this replacement mutant.

To analyze the effect of the MSD mutation in membrane fusion independent of other viral structural proteins, we used the Env expression vector. We found no significant difference in the steady-state amount of envelope proteins expressed on the cell surface and the CD4-binding efficiency (Fig. 5B). Therefore, the drastic changes in either trafficking or conformation cannot explain the observed prominent defect in fusion activity of GpA or VSV-G replacement mutants. One of the potential defects of membrane fusion in our MSD^{rep} mutants should reside in the post-CD4 binding step(s) of membrane fusion processes. In MSD^{rep} mutants, there may be a difference in the interactions between Env and the chemokine receptors or in the conformational changes induced after such interactions.

The exact defective steps in the membrane fusion mechanism of MSD^{rep} mutants remain to be determined. There should be a defect before the lipid dye mixing step, because we observed decreased efficiency of lipid dye transfer in MSD^{rep} mutants (Fig. 6B). We did not observe the discrepancy between lipid dye (CM-DiI) and cytoplasmic dye (Calecein blue, AM) transfer; therefore, there was no arrest in the hemifusion step. Recently, Lin and coworkers reported that truncating the MSD of simian immunodeficiency virus (SIV) decreased fusion activity (18). As with our mutants, their SIV Env mutants exhibited an overall decrease in lipid dye transfer as well as in cytoplasmic dye transfer. Theirs, however, showed a further downstream defect, namely, an enlargement of the fusion pore

induced by mutated Env. This was suggested by the difference in the efficiency of transfer between low-molecular-weight molecules (Calcein blue, AM) and larger molecules (enhanced blue fluorescent protein). We did not observe this difference in our assay. They also observed the gap between the lipid dye transfer and luciferase transfer assays. In our mutants, the decrease in the lipid dye transfer correlated well with the decrease in the transfer of T7 RNApol assay (Fig. 6B and C). The discrepancy between the studies might arise from the differences between the two viruses (SIV and HIV) or from the nature of the mutations introduced (truncation versus replacement).

We observed a pore formation efficiency of approximately 40% for the MSD^{rep} mutants compared with that observed with the WT despite their prominent fusion defect observed in MAGI cells. Because the two assays described in Fig. 3 and 6 employed different cell types and expression systems, it may be difficult to compare these two assays directly. There is the possibility that the discrepancy between the assays was artificially enhanced by the differences in the two assay systems. For example, the levels of expressed Env and of CD4 were higher in the T7 RNApol transfer assay than in the MAGI cell assay (data not shown). When a higher CD4-expressing cell line was used in the fusion assay instead of the MAGI cells, while maintaining with the provirus constructs, the efficiency of fusion was increased (data not shown). When the provirus constructs were used instead of the Env expression vectors in the T7 RNApol transfer assay, the values for pore formation were slightly decreased. The individual values of GpA, GpAG83I, and VSV-G were 39, 27, and 20%, respectively. The value for the mock treatment was about 1%. Thus, the observed gap could be accounted for in part by the difference in assay systems. However, very inefficient formation of the large syncytia in MSD^{rep} mutants might indeed suggest the presence of the defect in the steps after the formation of initial fusion pores.

Our data on MSD^{rep} mutants clearly demonstrate that not all heterologous MSDs can replace the gp41 MSD without affecting its function. The data indicate that the expression or retention of gp41 on the lipid bilayer and the fusion activity itself are rather independent functions. Our results also show that the mere maintenance of the GXXXG motif is not sufficient for fusion activity. It seems likely that a context-dependent arrangement of the glycine and other amino acid residues within the MSD is critical for functional integrity.

In this study, we have provided evidence that the MSD of gp41 affects the biogenesis of Env and also plays a critical role in membrane fusion for HIV-1. As our results for the Gly^{sub} and MSD^{rep} mutants suggest, the gp41 MSD shows a rather high tolerance for mutation but does require the MSD to have some specific sequences—or structures generated by them—for its proper function. One possible scenario is that the gp41 MSD may interact with some lipid or protein components during membrane fusion. Such an interaction between Env and lipid or protein moieties has been reported for the Semliki Forest virus and the influenza virus, respectively (2, 19). The gp41 MSDs might interact among themselves, with fusion peptides, or with the MSDs of other host proteins, such as CD4 or chemokine receptors, that are thought to come within close proximity of one another during the membrane fusion process. A failure to properly interact because of mutations in the gp41 MSD may affect the fusion process. To address these issues, additional systematic mutagenesis studies are needed to determine the critical residues of the MSD. Such studies should shed light on the molecular mechanisms of membrane fusion. Elucidating the precise molecular mechanism of membrane fusion—and the role of the gp41 MSD in it—may provide another target for a molecular intervention in HIV-1 infection.

ACKNOWLEDGMENTS

This study was supported by the Health and Labour Sciences Research Grants from Japanese Ministry of Health, Labor, and Welfare.

We thank A. M. Menting for assistance in manuscript preparation.

REFERENCES

1. **Aoki, Y., H. Aizaki, T. Shimoike, H. Tani, K. Ishii, I. Saito, Y. Matsuura, and T. Miyamura.** 1998. A human liver cell line exhibits efficient translation of HCV RNAs produced by a recombinant adenovirus expressing T7 RNA polymerase. Virology **250**:140–150.
2. **Armstrong, R. T., A. S. Kushnir, and J. M. White.** 2000. The transmembrane domain of influenza hemagglutinin exhibits a stringent length requirement to support the hemifusion to fusion transition. J. Cell Biol. **151**:425–437.
3. **Bosch, V., and M. Pawlita.** 1990. Mutational analysis of the human immunodeficiency virus type 1 *env* gene product proteolytic cleavage site. J. Virol. **64**:2337–2344.
4. **Bullough, P. A., F. M. Hughson, J. J. Skehel, and D. C. Wiley.** 1994. Structure of influenza haemagglutinin at the pH of membrane fusion. Nature **371**:37–43.
5. **Chan, D. C., D. Fass, J. M. Berger, and P. S. Kim.** 1997. Core structure of gp41 from the HIV envelope glycoprotein. Cell **89**:263–273.
6. **Chen, J., S. A. Wharton, W. Weissenhorn, L. J. Calder, F. M. Hughson, J. J. Skehel, and D. C. Wiley.** 1995. A soluble domain of the membrane-anchoring chain of influenza virus hemagglutinin (HA2) folds in *Escherichia coli* into the low-pH-induced conformation. Proc. Natl. Acad. Sci. USA **92**:12205–12209.
7. **Chesebro, B., and K. Wehrly.** 1988. Development of a sensitive quantitative focal assay for human immunodeficiency virus infectivity. J. Virol. **62**:3779–3788.
8. **Cleverley, D. Z., and J. Lenard.** 1998. The transmembrane domain in viral fusion: essential role for a conserved glycine residue in vesicular stomatitis virus G protein. Proc. Natl. Acad. Sci. USA **95**:3425–3430.
9. **Dubay, J. W., S. J. Roberts, B. H. Hahn, and E. Hunter.** 1992. Truncation of the human immunodeficiency virus type 1 transmembrane glycoprotein cytoplasmic domain blocks virus infectivity. J. Virol. **66**:6616–6625.
10. **Eisenberg, D., and M. Wesson.** 1990. The most highly amphiphilic alpha-helices include two amino acid segments in human immunodeficiency virus glycoprotein 41. Biopolymers **29**:171–177.
11. **Fass, D., S. C. Harrison, and P. S. Kim.** 1996. Retrovirus envelope domain at 1.7 angstrom resolution. Nat. Struct. Biol. **3**:465–469.
12. **Fleming, K. G., and D. M. Engelman.** 2001. Specificity in transmembrane helix-helix interactions can define a hierarchy of stability for sequence variants. Proc. Natl. Acad. Sci. USA **98**:14340–14344.
13. **Freed, E. O., and M. A. Martin.** 1996. Domains of the human immunodeficiency virus type 1 matrix and gp41 cytoplasmic tail required for envelope incorporation into virions. J. Virol. **70**:341–351.
14. **Harman, A., H. Browne, and T. Minson.** 2002. The transmembrane domain and cytoplasmic tail of herpes simplex virus type 1 glycoprotein H play a role in membrane fusion. J. Virol. **76**:10708–10716.
15. **Kemble, G. W., T. Danieli, and J. M. White.** 1994. Lipid-anchored influenza hemagglutinin promotes hemifusion, not complete fusion. Cell **76**:383–391.
16. **Kimpton, J., and M. Emerman.** 1992. Detection of replication-competent and pseudotyped human immunodeficiency virus with a sensitive cell line on the basis of activation of an integrated -galactosidase gene. J. Virol. **66**: 2232–2239.
17. **Kuiken, C., B. Foley, B. Hahn, P. Marx, F. McCutchan, J. Mellors, S. Wolinsky, and B. Korber.** 2001. HIV Sequence Compendium 2001. Theoretical Biology and Biophysics Group, Los Alamos National Laboratory, Los Alamos, N.M.
18. **Lin, X., C. A. Derdeyn, R. Blumenthal, J. West, and E. Hunter.** 2003. Progressive truncations C terminal to the membrane-spanning domain of simian immunodeficiency virus Env reduce fusogenicity and increase concentration dependence of Env for fusion. J. Virol. **77**:7067–7077.
19. **Lu, Y. E., T. Cassese, and M. Kielian.** 1999. The cholesterol requirement for Sindbis virus entry and exit and characterization of a spike protein region involved in cholesterol dependence. J. Virol. **73**:4272–4278.
20. **Malashkevich, V. N., B. J. Schneider, M. L. McNally, M. A. Milhollen, J. X. Pang, and P. S. Kim.** 1999. Core structure of the envelope glycoprotein GP2 from Ebola virus at 1.9-A resolution. Proc. Natl. Acad. Sci. USA **96**:2662–2667.

21. **Matsuda, Z., X. Yu, Q. C. Yu, T. H. Lee, and M. Essex.** 1993. A virion-specific inhibitory molecule with therapeutic potential for human immunodeficiency virus type 1. Proc. Natl. Acad. Sci. USA **90**:3544–3548.
22. **Melikyan, G. B., S. Lin, M. G. Roth, and F. S. Cohen.** 1999. Amino acid sequence requirements of the transmembrane and cytoplasmic domains of influenza virus hemagglutinin for viable membrane fusion. Mol. Biol. Cell. **10**:1821–1836.
23. **Melikyan, G. B., R. M. Markosyan, M. G. Roth, and F. S. Cohen.** 2000. A point mutation in the transmembrane domain of the hemagglutinin of influenza virus stabilizes a hemifusion intermediate that can transit to fusion. Mol. Biol. Cell **11**:3765–3775.
24. **Mendrola, J. M., M. B. Berger, M. C. King, and M. A. Lemmon.** 2002. The single transmembrane domains of ErbB receptors self-associate in cell membranes. J. Biol. Chem. **277**:4704–4712.
25. **Miller, M. A., R. F. Garry, J. M. Jaynes, and R. C. Montelaro.** 1991. A structural correlation between lentivirus transmembrane proteins and natural cytolytic peptides. AIDS Res. Hum. Retrovir. **7**:511–519.
26. **Mingarro, I., P. Whitley, M. A. Lemmon, and G. von Heijne.** 1996. Ala-insertion scanning mutagenesis of the glycophorin A transmembrane helix: a rapid way to map helix-helix interactions in integral membrane proteins. Protein Sci. **5**:1339–1341.
27. **Murakami, T., S. Ablan, E. O. Freed, and Y. Tanaka.** 2004. Regulation of human immunodeficiency virus type 1 Env-mediated membrane fusion by viral protease activity. J. Virol. **78**:1026–1031.
28. **Odell, D., E. Wanas, J. Yan, and H. P. Ghosh.** 1997. Influence of membrane anchoring and cytoplasmic domains on the fusogenic activity of vesicular stomatitis virus glycoprotein G. J. Virol. **71**:7996–8000.
29. **Op De Beeck, A., R. Montserret, S. Duvet, L. Cocquerel, R. Cacan, B. Barberot, M. Le Maire, F. Penin, and J. Dubuisson.** 2000. The transmembrane domains of hepatitis C virus envelope glycoproteins E1 and E2 play a major role in heterodimerization. J. Biol. Chem. **275**:31428–31437.
30. **Ory, D. S., B. A. Neugeboren, and R. C. Mulligan.** 1996. A stable human-derived packaging cell line for production of high titer retrovirus/vesicular stomatitis virus G pseudotypes. Proc. Natl. Acad. Sci. USA **93**:11400–11406.
31. **Owens, R. J., C. Burke, and J. K. Rose.** 1994. Mutations in the membrane-spanning domain of the human immunodeficiency virus envelope glycoprotein that affect fusion activity. J. Virol. **68**:570–574.
32. **Piller, S. C., J. W. Dubay, C. A. Derdeyn, and E. Hunter.** 2000. Mutational analysis of conserved domains within the cytoplasmic tail of gp41 from human immunodeficiency virus type 1: effects on glycoprotein incorporation and infectivity. J. Virol. **74**:11717–11723.
33. **Pincus, S. H., K. Wehrly, and B. Chesebro.** 1989. Treatment of HIV tissue culture infection with monoclonal antibody-ricin A chain conjugates. J. Immunol. **142**:3070–3075.
34. **Russ, W. P., and D. M. Engelman.** 2000. The GxxxG motif: a framework for transmembrane helix-helix association. J. Mol. Biol. **296**:911–919.
35. **Salzwedel, K., P. B. Johnston, S. J. Roberts, J. W. Dubay, and E. Hunter.** 1993. Expression and characterization of glycophospholipid-anchored human immunodeficiency virus type 1 envelope glycoproteins. J. Virol. **67**: 5279–5288.
36. **Shmulevitz, M., J. Salsman, and R. Duncan.** 2003. Palmitoylation, membrane-proximal basic residues, and transmembrane glycine residues in the reovirus p10 protein are essential for syncytium formation. J. Virol. **77**:9769–9779.
37. **Tan, K., J. Liu, J. Wang, S. Shen, and M. Lu.** 1997. Atomic structure of a thermostable subdomain of HIV-1 gp41. Proc. Natl. Acad. Sci. USA **94**: 12303–12308.
38. **Taylor, G. M., and D. A. Sanders.** 1999. The role of the membrane-spanning domain sequence in glycoprotein-mediated membrane fusion. Mol. Biol. Cell **10**:2803–2815.
39. **Ulmschneider, M. B., and M. S. Sansom.** 2001. Amino acid distributions in integral membrane protein structures. Biochim. Biophys. Acta **1512**:1–14.
40. **Venable, R. M., R. W. Pastor, B. R. Brooks, and F. W. Carson.** 1989. Theoretically determined three-dimensional structures for amphipathic segments of the HIV-1 gp41 envelope protein. AIDS Res. Hum. Retrovir. **5**:7–22.
41. **Vincent, M. J., N. U. Raja, and M. A. Jabbar.** 1993. Human immunodeficiency virus type 1 Vpu protein induces degradation of chimeric envelope glycoproteins bearing the cytoplasmic and anchor domains of CD4: role of the cytoplasmic domain in Vpu-induced degradation in the endoplasmic reticulum. J. Virol. **67**:5538–5549.
42. **Weiss, C. D., and J. M. White.** 1993. Characterization of stable Chinese hamster ovary cells expressing wild-type, secreted, and glycosylphosphatidylinositol-anchored human immunodeficiency virus type 1 envelope glycoprotein. J. Virol. **67**:7060–7066.
43. **Weissenhorn, W., A. Carfi, K. H. Lee, J. J. Skehel, and D. C. Wiley.** 1998. Crystal structure of the Ebola virus membrane fusion subunit, GP2, from the envelope glycoprotein ectodomain. Mol. Cell **2**:605–616.
44. **Weissenhorn, W., A. Dessen, S. C. Harrison, J. J. Skehel, and D. C. Wiley.** 1997. Atomic structure of the ectodomain from HIV-1 gp41. Nature **387**: 426–430.
45. **Wilk, T., T. Pfeiffer, A. Bukovsky, G. Moldenhauer, and V. Bosch.** 1996. Glycoprotein incorporation and HIV-1 infectivity despite exchange of the gp160 membrane-spanning domain. Virology **218**:269–274.
46. **Yu, X., X. Yuan, M. F. McLane, T. H. Lee, and M. Essex.** 1993. Mutations in the cytoplasmic domain of human immunodeficiency virus type 1 transmembrane protein impair the incorporation of Env proteins into mature virions. J. Virol. **67**:213–221.

J. Antibiot. 58(1): 65–68, 2005

NOTE

THE JOURNAL OF ANTIBIOTICS

Fungal Phenalenones Inhibit HIV-1 Integrase

Kazuro Shiomi, Ryosuke Matsui, Miki Isozaki, Harumi Chiba, Takahiro Sugai, Yuichi Yamaguchi, Rokuro Masuma, Hiroshi Tomoda, Tomoko Chiba, Hua Yan, Yoshihiro Kitamura, Wataru Sugiura, Satoshi Ōmura, Haruo Tanaka

Received: September 7, 2004 / Accepted: November 27, 2004

Abstract A phenalenone compound, atrovenetinone methyl acetal, was isolated from a culture broth of *Penicillium* sp. FKI-1463 as an HIV-1 integrase inhibitor, and it showed anti-HIV activity *in vitro*. HIV-1 integrase inhibition and anti-HIV activity of two other natural phenalenones were also studied. Among the tested compounds, funalenone inhibited HIV-1 integrase with an IC_{50} value of 10 μM and showed the best selectivity (anti-HIV, IC_{50}=1.7 μM; cytotoxicity, IC_{50}=87 μM).

Keywords: enzyme inhibitor, HIV interase, AIDS, phenalenone

Combined therapeutic regimens with reverse transcriptase inhibitors and protease inhibitors lead to a suppression of human immunodeficiency virus-1 (HIV-1) replication, reduction of viral load, and decline in morbidity and mortality [1, 2]. However, the therapy sometimes fails due to the emergence of mutant viruses that are resistant to these drugs [3]. Thus, it is critical to discover more effective and less toxic anti-HIV agents with different molecular targets in the viral replication cycle. We have previously screened microbial metabolites for new anti-HIV antibiotics that inhibit entry of HIV-1 into the susceptive cells, and found isochromophilones and chloropeptins by a gp120-sCD4 binding assay [4, 5] and actinohivin by a syncytium formation assay [6]. There are three viral enzymes essential for HIV-1 replication, reverse transcriptase, protease, and integrase. Of these, only integrase has not been the target of a clinically used inhibitor. HIV DNA is inserted into the host genome by a specialized DNA recombination reaction in which the viral integrase is the key player [7, 8]. The integration reaction is composed of three steps, 3′-processing, strand transfer, and gap filling, and integrase catalyses the first and second steps. The third step is thought to be catalyzed by cellular enzymes. Many natural and synthetic integrase inhibitors have been reported [8~12] but only a few compounds show high selectivity. Therefore, we screened microbial metabolites for HIV-1 integrase inhibitors, and found that a culture broth of *Penicillium* sp. FKI-1463 has the inhibitory

H. Tanaka (Corresponding author), **K. Shiomi, R. Matsui, M. Isozaki, H. Chiba, T. Sugai:** School of Pharmaceutical Sciences Kitasato University, 5-9-1 Shirokane, Minato-ku, Tokyo 108-8641, Japan, E-mail: tanakah@pharm.kitasato-u.ac.jp

Y. Yamaguchi, R. Masuma, H. Tomoda, S. Ōmura: The Kitasato Institute, 5-9-1 Shirokane, Minato-ku, Tokyo 108-8641, Japan

R. Masuma, H. Tomoda, S. Ōmura: Kitasato Institute for Life Sciences, Kitasato University, 5-9-1 Shirokane, Minato-ku, Tokyo 108-8641, Japan

T. Chiba, H. Yan, W. Sugiura: AIDS Research Center, National Institute of Infectious Diseases, 4-7-1 Gakuen, Musashimurayama-shi, Tokyo 208-0011, Japan

Y. Kitamura: Advanced Clinical Research Center, Institute of Medical Science, The University of Tokyo, 4-6-1 Shirokanedai, Minato-ku, Tokyo 108-8639, Japan

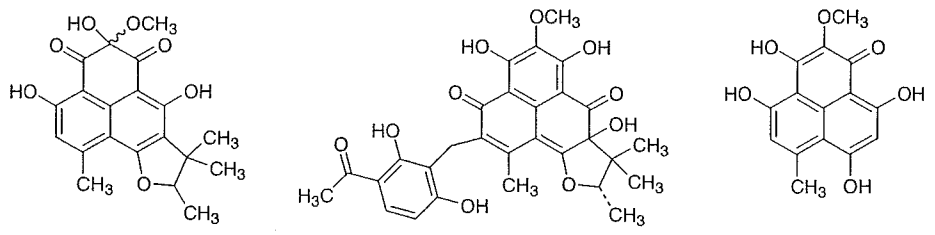

Atrovenetinone methyl acetal (**1**) Erabulenol B (**4**) Funalenone (**5**)

Fig. 1 Natural phenalenones.

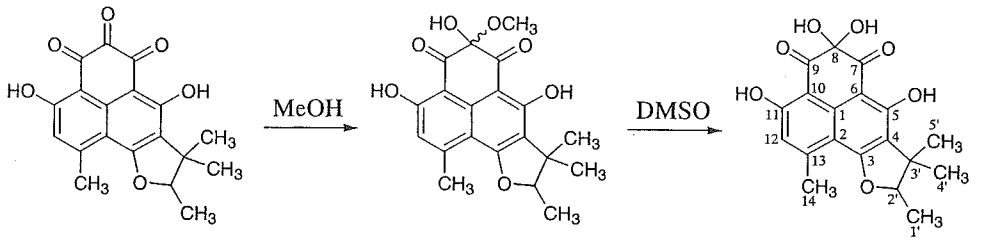

2 **1** **3**

Fig. 2 Conversion of atrovenetinone.

activity. The active compound was identified as a phenalenone compound, atrovenetinone methyl acetal (**1**, Fig. 1) [13]. This paper presents integrase-inhibiting and anti-HIV activities of **1** and other natural phenalenones.

A slant culture of the strain FKI-1463 grown on YpSs agar was inoculated into a 500-ml Erlenmeyer flask containing 100 ml of a seed medium consisting of glucose 2.0%, Polypepton (Nihon Pharmaceutical Co.) 0.5%, yeast extract 0.2% (Oriental Yeast Co.), KH_2PO_4 0.1%, $MgSO_4 \cdot 7H_2O$ 0.05%, and agar 0.1%, pH 6.0. It was cultured on a reciprocal shaker at 27°C for 3 days. One milliliter of the seed culture was transferred into each of twenty 500-ml Erlenmeyer flasks containing 100 ml of a production medium consisting of glycerol 3.0%, oatmeal (Nihon Shokuhin Seizo Co.) 2.0%, dry yeast (Gist-brocades) 1.0%, KH_2PO_4 1.0%, Na_2HPO_4 1.0%, $MgSO_4 \cdot 7H_2O$ 0.5%, pH not adjusted. The fermentation was carried out on a reciprocal shaker at 27°C for 7 days. The cultured broth (2.0 liters) was centrifuged and the mycelia were extracted with methanol, which was then removed from the extract by evaporation. The aqueous extract was partitioned with ethyl acetate at pH 3.0, and the organic layer was concentrated to dryness *in vacuo* to afford brown oil (644 mg). This was chromatographed over a silica gel column. Active fractions, eluted with $CHCl_3$-methanol (100 : 1) and $CHCl_3$-methanol (20 : 1), were concentrated to yield a crude material (284 mg). It was applied on a ODS silica gel column and eluted with aqueous CH_3CN. The 50% CH_3CN eluates were concentrated (95.5 mg) and chromatographed over Sephadex LH-20 to yield green oil (86.8 mg). It was further purified by reverse phase (Pegasil ODS, Senshu Scientific Co.) and normal phase (Pegasil Silica, Senshu Scientific Co.) HPLC to yield 50.5 mg of green oil.

The purified compound was implicated as **1** by comparison of the NMR data in $CDCl_3$ with the reported data by Nakanishi *et al.* [13]. Atrovenetinone (**2**) is easily converted into an acetal in alcohol (Fig. 2) [14], and the acetal is a mixture of diastereomers [13]. So, the NMR spectra of **1** are complicated. Since **2** exists as the hydrate (**3**) in DMSO [14], we observed the NMR spectra of the isolated compound in DMSO-d_6. The spectra were simplified, and each signal was assigned as follows: ^{1}H NMR (600 MHz) δ 13.67 (1H, s, 5-OH), 12.92 (1H, s, 11-OH), 6.86 (1H, s, 12-H), 4.70 (1H, q, J=6.5 Hz, 2′-H), 4.04 (1H, br s, 8-OH), 2.72 (3H, s, 14-H_3), 1.45 (3H, s, 5′-H_3), 1.22 (3H, s, 4′-H_3), 1.41 (3H, d, J=6.5 Hz, 1′-H_3); ^{13}C NMR (150 MHz) δ 197.7 (C-7), 196.2 (C-9), 165.1 (C-11), 164.8 (C-3), 164.5 (C-5), 147.9 (C-13), 136.7 (C-1), 118.1 (C-4), 117.6 (C-12), 109.0 (C-2), 104.9 (C-10), 101.9 (C-6), 91.1 (C-2′), 88.0 (C-8), 42.8 (C-3′), 25.2 (C-5′), 23.5 (C-14), 20.4 (C-4′), 14.3 (C-1′). The NMR data suggested that **1** was converted into **3** in DMSO solution (Fig. 2), and released methanol signals (δ_H 3.15 and δ_C 48.6) were also

Table 1 Biological activities of phenalenones

	IC_{50} (μM)			Selectivity (B/A)
	HIV-1 integrase inhibition	Anti-HIV activity (A)	Cytotoxicity (HPB-M(a)[a]) (B)	
Atrovenetinone methyl acetal (**1**)	19	6.7	13	1.9
Erabulenol B (**4**)	7.9	17	230	14
Funalenone (**5**)	10	1.7	87	51

[a] HPB-M(a) cells are human peripheral blood cells transformed by murine leukemia virus. Anti-HIV activity was measured using HPB-M(a) cells with LTR driven luciferase.

observed. Thus, the isolated compound was identified as **1**. It has been reported as a myosin light chain kinase inhibitor isolated from a culture broth of *Penicillium* sp. It may be derived from **2** during purification. Compound **2** is a phenalenone compound originally obtained by the oxidation of atrovenetin produced by *Penicillium* sp., and **2** was lately isolated from a culture broth of *Gremmeniella abietina* [14, 15].

We have previously isolated the other fungal phenalenones, erabulenol B (**4**) which inhibits cholesteryl ester transfer protein and funalenone (**5**) which inhibits collagenase [16, 17]. Funalenone was also reported to inhibit bacterial cell wall synthesis enzymes MraY and MurG [18]. We evaluated integrase inhibition and anti-HIV activity of **1** together with those phenalenones. HIV-1 integrase activity was measured by strand transfer assay according to Craigie *et al.* [7]. *In vitro* anti-HIV activities of the test compounds were measured by originally established reporter human T cell line with LTR driven luciferase. The cells were infected with wild type HIV-1, and the compounds were added at different concentrations ranging from 0.0016 to 125 μg/ml. Luciferase activities of the cells, which appeared to correlate with the level of HIV-1 replication, were measured at day 7, and anti-HIV IC_{50}s of the compounds were evaluated. The IC_{50} value of **1** against integrase was 19 μM, and it also showed anti-HIV activity at 6.7 μM (Table 1). However, its cytotoxicity was relatively high. Compounds **4** and **5** showed more potent inhibition against integrase than **1**, and also exhibited anti-HIV activity. The anti-HIV activity of **5** was the most potent (1.7 μM), and its cytotoxicity (87 μM) was lower than **1**. Though **5** was reported to inhibit collagenase and bacterial cell wall synthesis enzymes [17, 18], those inhibitions were less potent than the integrase inhibition and anti-HIV activity. Therefore, **5** may be a good candidate lead compound for anti-HIV agent. Inhibition of DNA polymerases by the other phenalenones have been reported, but they did not inhibit HIV reverse transcriptase [19]. A plant metabolite, hypericin [20], is the only *ortho*- and *peri*-fused aromatic compound reported to show integrase inhibition [21].

Acknowledgements We are grateful to Dr. Junji Inokoshi, School of Pharmaceutical Sciences, Kitasato University for providing funalenone. This work was supported in part by the Grant of Research for the Development of Anti-AIDS Pharmaceutical Products (KA12505), Japan Health Sciences Foundation, and the 21st Century COE Program, Ministry of Education, Culture, Sports, Science, and Technology.

References

1. Hogg RS, Rhone SA, Yip B, Sherlock C, Conway B, Schechter MT, O'Shaughnessy MV, Montaner JSG. Antiviral effect of double and triple drug combinations amongst HIV-infected adults: lessons from the implementation of viral load-driven antiretroviral therapy. AIDS 12: 279–284 (1998)
2. Palella FJ Jr, Delaney KM, Moorman AC, Loveless MO, Fuhrer J, Satten GA, Aschman DJ, Holmberg SD. Declining morbidity and mortality among patients with advanced human immunodeficiency virus infection. N Engl J Med 338: 853–860 (1998)
3. Deeks SG. Treatment of antiretroviral-drug-resistant HIV-1 infection. Lancet 362: 2002–2011 (2003)
4. Matsuzaki K, Ikeda H, Masuma R, Tanaka H, Ōmura S. Isochromophilones I and II, novel inhibitors against gp120-CD4 binding produced by *Penicillium multicolor* FO-2338. I. Screening, taxonomy, fermentation, isolation and biological activity. J Antibiot 48: 703–707 (1995)
5. Tanaka H, Matsuzaki K, Nakashima H, Ogino T, Matsumoto

A, Ikeda H, Woodruff HB, Ōmura S. Chloropeptins, new anti-HIV antibiotics inhibiting gp120-CD4 binding from *Streptomyces* sp. 1. Taxonomy, fermentation, isolation, physico-chemical properties and biological activities. J Antibiot 50: 58–65 (1997)

6. Chiba H, Inokoshi J, Okamoto M, Asanuma S, Matsuzaki K, Iwama M, Mizumoto K, Tanaka H, Oheda M, Fujita K, Nakashima H, Shinose M, Takahashi Y, Ōmura S. Actinohivin, a novel anti-HIV protein from an actinomycete that inhibits syncytium formation: isolation, characterization, and biological activities. Biochem Biophys Res Commun 282: 595–601 (2001)
7. Craigie R, Hickman AB, Engelman A. Integrase. *In* HIV. Volume 2. *Ed.*, Karn J, pp. 53–71, IRL Press, Oxford (1995)
8. Pommier Y, Neamati N. Inhibitors of human immunodeficiency virus integrase. *In* Advances in Virus Research. Volume 52. *Ed.*, Maramorosch K *et al.*, pp. 427–458, Academic Press, San Diego (1999)
9. Cos P, Maes L, Vanden Berghe D, Hermans N, Pieters L, Vlietinck A. Plant substances as anti-HIV agents selected according to their putative mechanism of action. J Nat Prod 67: 284–293 (2004)
10. Hazuda D, Blau CU, Felock P, Hastings J, Pramanik B, Wolfe A, Bushman F, Farnet C, Goetz M, Williams M, Silverman K, Lingham R, Singh S. Isolation and characterization of novel human immunodeficiency virus integrase inhibitors from fungal metabolites. Antivir Chem Chemother 10: 63–70 (1999)
11. Singh SB, Jayasuriya H, Dewey R, Polishook JD, Dombrowski AW, Zink DL, Guan Z, Collado J, Platas G, Pelaez F, Felock PJ, Hazuda DJ. Isolation, structure, and HIV-1 integrase inhibitory activity of structurally diverse fungal metabolites. J Ind Microbiol Biotechnol 30: 721–731 (2003)
12. Ondeyka JG, Zink DL, Dombrowski AW, Polishook JD, Felock PJ, Hazuda DJ, Singh SB. Isolation, structure and HIV-1 integrase inhibitory activity of exophillic acid, a novel fungal metabolite from *Exophiala pisciphila*. J Antibiot 56: 1018–1023 (2003)
13. Nakanishi S, Toki S, Saitoh Y, Tsukuda E, Kawahara K, Ando K, Matsuda Y. Isolation of myosin light chain kinase inhibitors from microorganisms: dehydroaltenusin, altenusin, atrovenetinone, and cyclooctasulfur. Biosci Biotechnol Biochem 59: 1333–1335 (1995)
14. Ayer WA, Hoyano Y, Pedras MS, van Altena I. Metabolites produced by the Scleroderris canker fungus, *Gremmeniella abietina*. Part 1. Can Chem 64: 1585–1589 (1986)
15. Narasimhachari N, Vining LC. Studies on the pigments of *Penicillium herquei*. Can J Chem 41: 641–648 (1963)
16. Tomoda H, Tabata N, Masuma R, Si SY, Ōmura S. Erabulenols, inhibitors of cholesteryl ester transfer protein produced by *Penicillium* sp. FO-5637. I. Production, isolation and biological properties. J Antibiot 51: 618–623 (1998)
17. Inokoshi J, Shiomi K, Masuma R, Tanaka H, Yamada H, Ōmura S. Funalenone, a novel collagenase inhibitor produced by *Aspergillus niger*. J Antibiot 52: 1095–1100 (1999)
18. Zawadzke LE, Wu P, Cook L, Fan L, Casperson M, Kishnani M, Calambur D, Hofstead SJ, Padmanabha R. Targeting the MraY and MurG bacterial enzymes for antimicrobial therapeutic intervention. Anal Biochem 314: 243–252 (2003)
19. Perpelescu M, Kobayashi J, Furuta M, Ito Y, Izuta S, Takemura M, Suzuki M, Yoshida S. Novel phenalenone derivatives from a marine-derived fungus exhibit distinct inhibition spectra against eukaryotic DNA polymerases. Biochemistry 41: 7610–7616 (2002)
20. Pace N, Mackinney G. Hypericin, the photodynamic pigment from St. John'swort. J Am Chem Soc 63: 2570–2574 (1941)
21. Farnet CM, Wang B, Hansen M, Lipford JR, Zalkow L, Robinson WE, Jr, Siegel J, Bushman F. Human immunodeficiency virus type 1 cDNA integration: new aromatic hydroxylated inhibitors and studies of the inhibition mechanism. Antimicrob Agents Chemother 42: 2245–2253 (1998)

BATCH: jp1a190 USER: lkr69 DIV: @xyv04/data1/CLS_pj/GRP_jp/JOB_i01/DIV_jp046860+ DATE: November 29, 2004

Resistant Mechanism against Nelfinavir of Human Immunodeficiency Virus Type 1 Proteases

Hirotaka Ode,* Masami Ota, Saburo Neya, Masayuki Hata, Wataru Sugiura,† and Tyuji Hoshino

Graduate School of Pharmaceutical Sciences, Chiba University, Chiba 263-8522, Japan

Received: July 15, 2004; In Final Form: October 12, 2004

Inhibitors against human immunodeficiency virus type-1 (HIV-1) proteases are finely effective for anti-HIV-1 treatments. However, the therapeutic efficacy is reduced by the rapid emergence of inhibitor-resistant variants of the protease. Among patients who failed in the inhibitor nelfinavir (NFV) treatment, D30N, N88D, and L90M mutations of HIV-1 protease are often observed. Despite the serious clinical problem, it is not clear how these mutations, especially nonactive site mutations N88D and L90M, affect the affinity of NFV or why they cause the resistance to NFV. In this study, we executed molecular dynamics simulations of the NFV-bound proteases in the wild-type and D30N, N88D, D30N/N88D, and L90M mutants. Our simulations clarified the conformational change at the active site of the protease and the change of the affinity with NFV for all of these mutations, even though the 88th and 90th residues are not located in the NFV-bound cavity and not able to directly interact with NFV. D30N mutation causes the disappearance of the hydrogen bond between the *m*-phenol group of NFV and the 30th residue. N88D mutation alters the active site conformation slightly and induces a favorable hydrophobic contact. L90M mutation dramatically changes the conformation at the flap region and leads to an unfavorable distortion of the binding pocket of the protease, although 90M is largely far apart from the flap region. Furthermore, the changes of binding energies of the mutants from the wild-type protease are shown to be correlated with the mutant resistivity previously reported by the phenotypic experiments.

Introduction

Replication of human immunodeficiency virus type 1 (HIV-1) requires the processing of gag and gag-pol polyprotein precursors by the virus-encoded aspartic protease, so-called HIV-1 protease.[1] Therefore, the protease has been one of the major targets of anti-HIV-1 treatments.[2] Today, seven protease inhibitors (PIs) are approved by the FDA and are available clinically. Those drugs are well-designed to fit the inside of the binding cavity, mimicking the configuration of a substrate in the transition state for the hydrolysis reaction by the protease.[3] However, HIV-1 frequently acquires the resistance to these inhibitors through specific mutations due to the high polymorphism and adaptability of the protease.[4−7] Serious resistant mutants survive during the treatment with PIs and cause a failure in long-term HIV chemotherapy.

Among patients who failed in the treatment with nelfinavir, NFV (Figure 1), which is one of the PIs, substitutions of asparagine (N) for aspartic acid (D) at codon 30 (D30N), aspartic acid for asparagine at codon 88 (N88D), and methionine (M) for leucine (L) at codon 90 (L90M) are frequently seen in HIV-1 protease.[8,9] D30N is a primary NFV-resistant mutation, which appears to be very specific for this inhibitor. N88D is an additional mutation to D30N. A combination of D30N and N88D is the most commonly seen in patients treated with NFV, and N88D compensates for the loss of replicative capacity resulting from D30N as a secondary mutation. L90M is a primary mutation responsible for the resistance to both NFV and saquinavir[10] and also appears to be associated with the resistance to the other PIs.[4−6] There are two evolutionarily possible pass ways for the NFV-related mutation acquisition, and the L90M acquisition pass way is evolutionarily different from the pass way of D30N.[11,12]

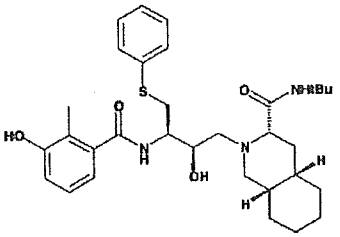

Figure 1. Structure of NFV. According to the crystal structure (PDB code: 1OHR), the *m*-phenol group of the 2-methyl-3-hydroxylbenzamide side chain of NFV interacts with 30D by hydrogen bonding in the S2 pocket of HIV-1 protease. The *tert*-butylcarboxamide moiety occupies the S2′ subsite, the S-phenyl group and dodecahydroisoquinoline ring fit into the hydrophobic S1 and S1′ pockets, and the central hydroxyl group is bound to the catalytic aspartates.

The three-dimensional X-ray structure of the NFV-bound protease[13] implies that D30N mutation would alter the direct electrostatic interaction with the *m*-phenol group of NFV at the active site (Figure 2). It is, however, difficult to understand the NFV resistance due to N88D or L90M mutations because these 88th and 90th residues are located at the nonactive site near the dimer interface. Recently, Mahalingam and co-workers determined some high-resolution X-ray crystal structures of D30N, N88D, or L90M mutants combined with peptide inhibitor analogues, not NFV,[14−16] and suggested the mechanism of the resistance. They found that D30N mutation altered the interac-

* Corresponding author. Tel.: +81-43-290-2926. Fax: +81-43-290-2925. E-mail: odehir@graduate.chiba-u.jp.

† AIDS Research Center, National Institute of Infectious Diseases, Musashimurayama, Tokyo 208-0011, Japan.

10.1021/jp046860+ CCC: $30.25
Published on Web 00/00/0000 PAGE EST: 9.5

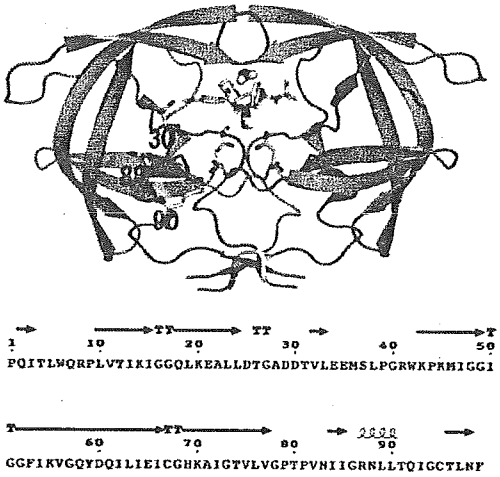

Figure 2. X-ray structure of the HIV-1 protease/NFV complex (PDB code: 1OHR). Locations of the two catalytic aspartates and the residues related with NFV resistance (30, 88, 90) are shown in the stick representation in one subunit of the protease dimer. The wild-type sequence is shown below.

tion with the inhibitors, N88D mutation lost the water that mediated hydrogen bond interactions among 31T, 74T, and 88D, and L90M caused an unfavorable van der Waals contact between 24T/25D and the long side chain of 90M. Further, they reported that L90M mutants altered the active site conformation when indinavir entered the binding cavity of the protease.[17] Though these structural features might be seen in the proteases complexed with NFV, a clear explanation on the resistance to NFV due to these mutations has not been provided yet.

Computational chemistry has been developed in recent years, and detailed analysis has been significantly improved. Many computational works were already carried out to clarify the catalytic mechanism of HIV-1 protease in its substrate-hydrolysis reaction.[18−30] And the other works discussed the drug-resistant mechanisms of some familiar active site mutations.[31−36] In the present study, we discussed the resistant mechanism of not only active site mutation D30N but also nonactive site mutations N88D, L90M. To clarify these mechanisms, we investigated the wild-type HIV-1 protease and D30N, N88D, D30N/N88D, and L90M mutants complexed with NFV on the basis of the molecular dynamics (MD) approach explicitly including the solvate condition. Our MD simulations for each mutant demonstrated the respective resistant mechanisms to NFV. Not only active site mutation D30N but also nonactive site mutations N88D and L90M affect the interaction between NFV and the protease through the structural modification of the binding cavity. There are no papers reported on the resistant mechanism of the nonactive site mutations through a computational approach. The atom-level understanding of the origins of these resistances will be useful in the design of better PIs. Further, our work suggests the possibility to reproduce the experimental phenotype data from the results of MD simulation.

Materials and Methods

MD Simulation. The reliability of MD simulations largely depends on the selection of force field parameters and the assignment of atomic charges. Hence, the electrostatic potential of NFV was preliminarily calculated at the B3LYP/6-31G(d, p) level using the Gaussian 98 program[37] after geometry optimization. The partial atom charges for NFV utilized in the MD simulation were determined using the RESP method[38] so that the atom charges could reproduce the values of the calculated electrostatic potential at the surrounding points of NFV. The charges were set equal between two atoms if they are the same element and have the same bond coordination. Afterward, all the minimizations and MD simulations were executed with the Sander module of AMBER 7 package.[39] The AMBER parm99 force field[40] was used as the parameters for the van der Waals and the bonded energy terms.

Each initial structure for the wild-type protease of clade B and D30N, N88D, D30N/N88D, and L90M mutants complexed with NFV was modeled on the basis of the coordinates of an X-ray crystal structure (PDB code: 1OHR)[13] using the LEaP module. All the crystal waters were included in each model. Each model was placed in a periodic cubic box filled with the about 8000 TIP3P water molecules.[41] The cutoff distance for the long-range electrostatic and the van der Waals terms was 12.0 Å. All covalent bonds to hydrogen atoms were constrained using the SHAKE algorithm.[42] Periodic boundary conditions were applied to avoid the edge effects in all calculations. Energy minimization was achieved via three stages. At first, the movement was allowed only for the water molecules. Next, the ligand and the mutated residues were allowed to move in addition to the water molecules. Last, all atoms were permitted to move freely. In each stage, energy minimization was executed by the steepest decent method for the first 1000 steps and the conjugated gradient method for the subsequent 3000 steps. The protonation states of the catalytic aspartates 25D/25′D were determined performing energy minimizations for all combinations of the protonation states (25D/25′D both protonated, 25D/25′D both unprotonated, 25D protonated and 25′D unprotonated, 25D unprotonated and 25′D protonated). The combination with protonated 25D and unprotonated 25′D showed the lowest total potential energy. This protonation state is consistent with the results of the previous work by Zoete et al.[43]

After a 24-ps heating calculation until 300 K using the NVT ensemble, MD simulations were executed using the NPT ensemble at 1 atm and at 300 K for more than 1 ns, with a basic time step of 1 fs. After a 500-ps equilibrating calculation, the MD simulations showed no large fluctuations (the deviation of the root-mean square deviation, RMSD, of the main chain is less than 0.1 Å in each model; more detailed data are shown in Supporting Information). Coordinates of 200 snapshots at the intervals of 0.5 ps were obtained as structural data; those were collected for the last 100 ps of the simulations.

Difference Distance Plot. The difference distance plots are drawn to assess the intermolecular relative shifts in response to the mutation. First, $C\alpha_i$-to-$C\alpha_j$ distances, $\mathbf{d}_{ij}^{\mathbf{A}}$, are computed for all the combinations of the Cα atoms in the protease of a mutant (A). Second, the same distances, $\mathbf{d}_{ij}^{\mathbf{B}}$, are measured for the wild-type model (B). The difference distances $\mathbf{d}_{ij}^{\mathbf{AB}}$ of the residues i and j are given by

$$\mathbf{D}_{ij}^{\mathbf{AB}} = |\mathbf{d}_{ij}^{\mathbf{A}} - \mathbf{d}_{ij}^{\mathbf{B}}|$$

Further, the error-scaled difference distance[44,45] $\mathbf{E}_{ij}^{\mathbf{AB}}$ is estimated by

$$\mathbf{E}_{ij}^{\mathbf{AB}} = \mathbf{D}_{ij}^{\mathbf{AB}} / \sigma(\mathbf{D}_{ij}^{\mathbf{AB}})$$

$$\sigma(\mathbf{D}_{ij}^{\mathbf{AB}}) = [(\sigma_{r,i}^{\mathrm{A}})^2 + (\sigma_{r,j}^{\mathrm{A}})^2 + (\sigma_{r,i}^{\mathrm{B}})^2 + (\sigma_{r,j}^{\mathrm{B}})^2]^{1/2}$$

where $\sigma_{r,i}^{\mathrm{A}}$ is the radial positional error that corresponds to the uncertainty for an individual atom position. The difference distance is plotted on the lower left panel, and the error-scaled

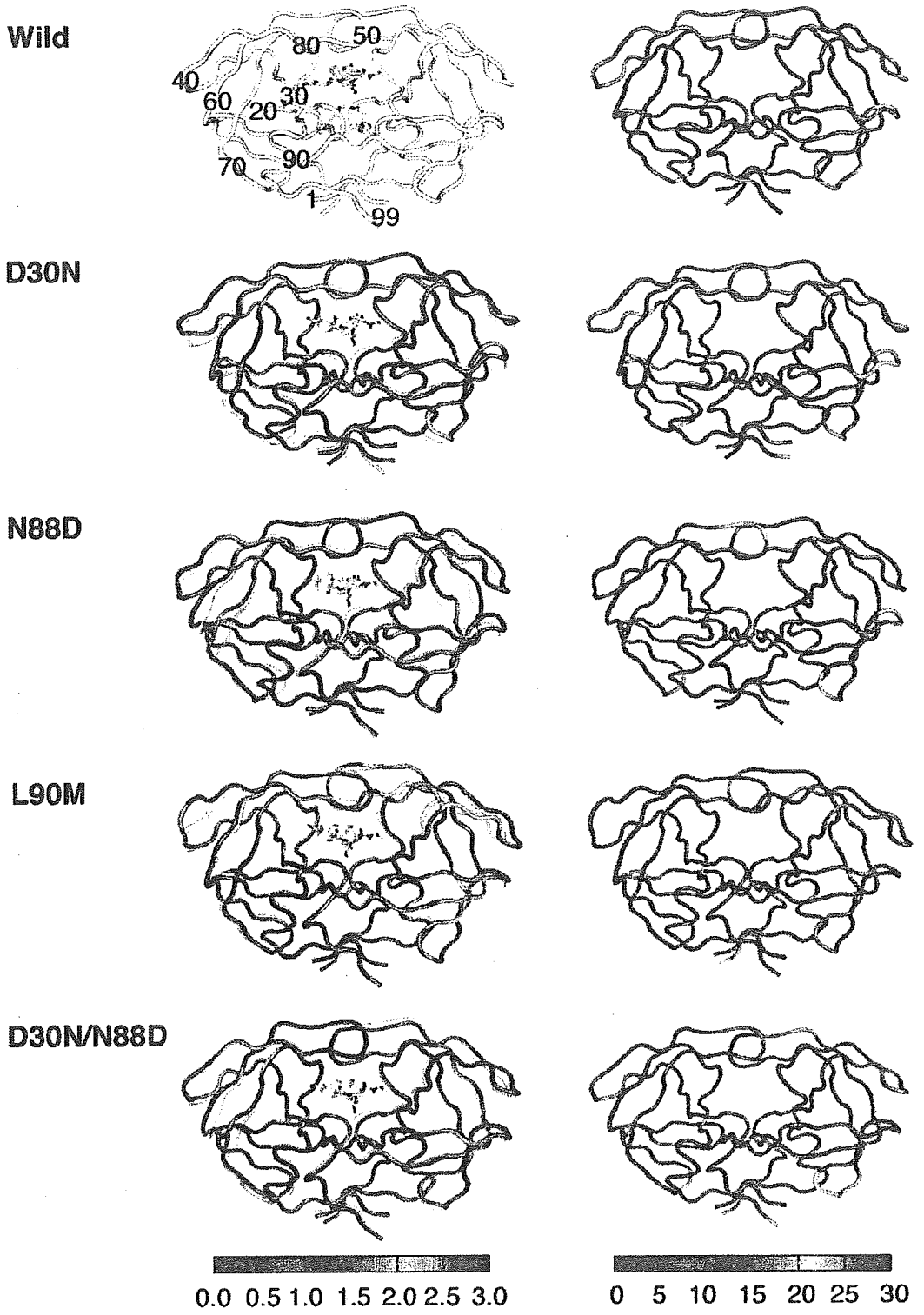

Figure 3. Left: Plots of RMSD between the average structures of the wild-type protease and each mutant, traced over every main chain atom. Each mutant structure is superimposed on the wild-type structure represented by white tubes. Right: B-factor values for main chain atoms in the wild-type and mutated proteases. The color represents the magnitude of the RMSD and B-factor shown at the lower bar. Scales are in units of angstroms and squared angstroms, respectively.

difference distance is on the upper right one in the two-dimensional map of Figure 4 as a function of residue numbers by using GNUPLOT.[46]

Hydrogen Bond Criterion. The formation of a hydrogen bond was defined in terms of distance and orientation. The combination of donor D, hydrogen H, and acceptor A atoms

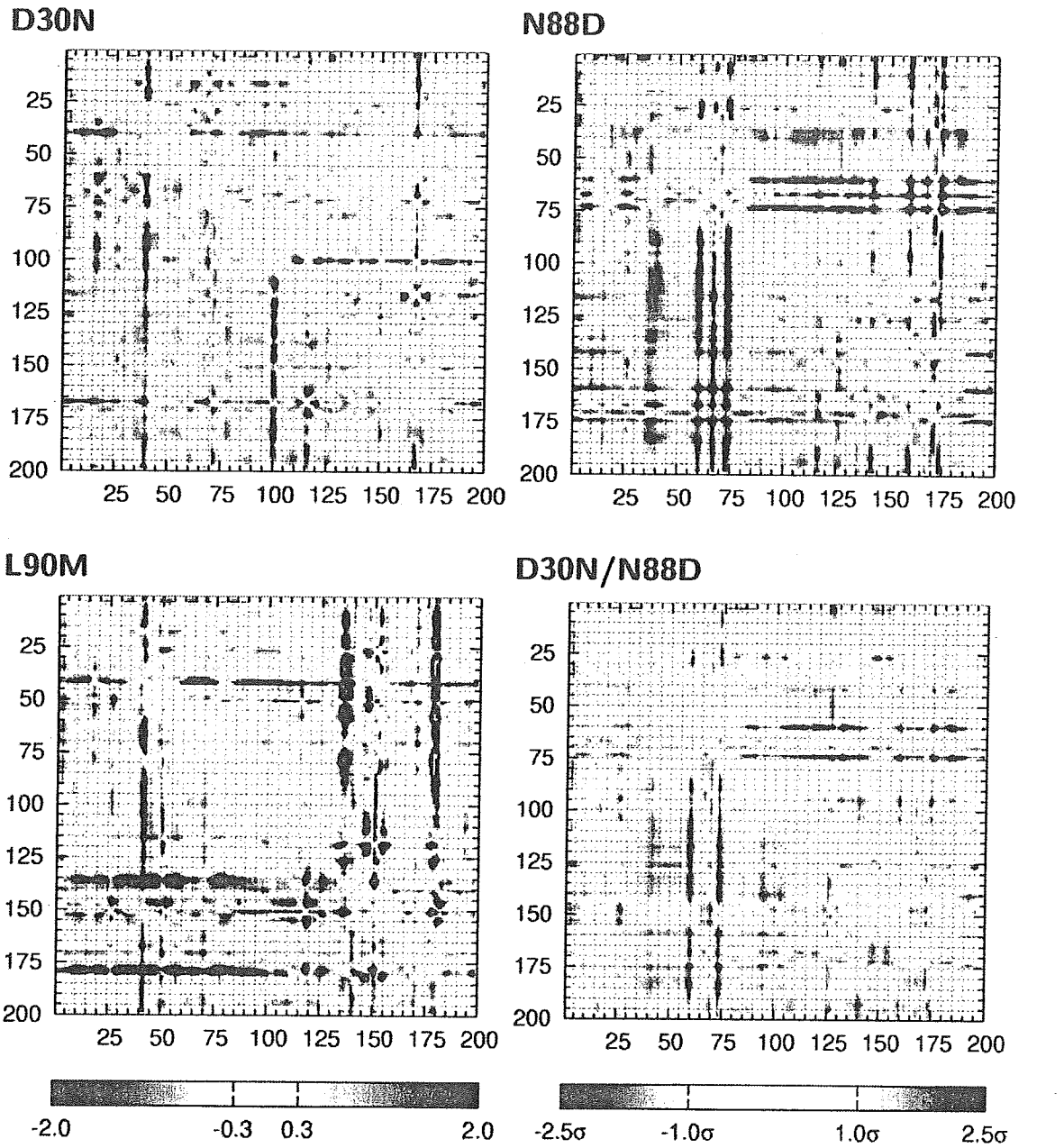

Figure 4. Difference distance matrixes and error-scaled difference matrixes for the Cα atoms. The difference distances for all pairs of residues in the protease are shown on the lower panel. The color represents the magnitude, as shown on the bar on the lower left. The upper right panel shows the error-scaled difference distance matrixes. Changes greater than 1.0σ and smaller than 2.5σ are colored as seen on the lower right bar. Numbers 1−99 represent the residues from 1P to 99F, and numbers 101−199 represents the residues from 1′P to 99′F.

with a D−H···A configuration is regarded as a hydrogen bond when the distance between donor D and acceptor A is shorter than R_{max} and the angle H−D−A is smaller than Θ_{max}. The values of 3.5 Å and 60.0° were adopted for R_{max} and Θ_{max} in this study.

Buried Surface Area (SA). The solvate accessible SA[47] was computed with Paul Beroza's molsurf program, which was based on the analytical technique primarily developed by Connolly[48] to evaluate the surface area buried by a ligand in binding to the enzyme. The SA is computed for the NFV-bound protease structure. SA is also calculated both for only NFV and for the free protease. The difference in SA values between the bound and the unbound cases is defined as the SA buried on complexation.[49]

Binding Energy Calculation. The binding free energy[50] is calculated on the basis of the next equation:

$$\Delta G_b = \Delta G_{MM} + \Delta G_{sol} - T\Delta S$$

where ΔG_b is the binding free energy in solution, ΔG_{MM} is the interaction energy between the ligand and the protein, ΔG_{sol} is the solvation energy, and $-T\Delta S$ is the conformational entropy contribution to the binding. When it is assumed that the entropies are almost the same in magnitude among the mutants, the